

## Fourier-transform photoluminescence spectroscopy of excitons bound to group-III acceptors in silicon: Zeeman effect

V. A. Karasyuk, M. L. W. Thewalt, and S. An

*Department of Physics, Simon Fraser University, Burnaby, British Columbia, Canada, V5A1S6*

E. C. Lightowers

*Physics Department, King's College London, Strand, London WC2R 2LS, United Kingdom*

A. S. Kaminskii

*Institute of Radioengineering and Electronics RAS, Mokhovaya 11, Moscow 103907, Russia*

(Received 22 April 1996; revised manuscript received 3 June 1996)

Photoluminescence of excitons bound to Al, Ga, In, and Tl acceptors in Si was studied at liquid-He temperatures in magnetic fields up to 14.5 T with  $\langle 001 \rangle$ ,  $\langle 111 \rangle$ , and  $\langle 110 \rangle$  orientations with 0.0025-meV spectral resolution. All details of the Zeeman spectra for every field orientation, with up to 30 resolved spectral components, have been explained on the basis of a simple model of acceptor bound excitons with holes in a singlet state  $J=0$ . The variation of the electron valley-orbit splitting of the bound exciton energy levels in magnetic fields was used for unambiguous identification of the zero-field valley-orbit state ordering. An additional 0.02-meV splitting of the  $\Gamma_5$  bound exciton energy levels due to spin-orbit coupling was observed for In bound excitons. The amplitude ratios in polarized Zeeman spectra agree with selection rules derived on the basis of the shell model. The ratios of the selection rule constants determined from the zero-field spectra indicate that hole scattering is responsible for no-phonon optical transitions in acceptor bound excitons. The electron spin and valley-orbit relaxation times were estimated to be longer than 3 ns and shorter than 76 ns on the basis of nonthermal population of the excited In and Tl bound exciton energy levels and complete thermalization of the Al and Ga bound excitons.

[S0163-1829(96)06035-3]

### I. INTRODUCTION

Photoluminescence (PL) spectroscopy of excitons bound to various defects is widely used for characterization of semiconductors.<sup>1</sup> Silicon was the first material in which bound excitons (BE's) were observed.<sup>2</sup> The bulk of the early BE studies in Si was carried out using grating spectrometers with a spectral resolution of up to 0.1 meV.<sup>3</sup> These studies confirmed, in particular, that an exciton bound to a neutral acceptor ( $A^0X$ , where  $A$  stands for a particular acceptor species) can be treated as a complex consisting of two holes and an electron bound to a negatively charged acceptor ion ( $A^-$ ). Holes at the top of the valence band have an approximate angular momentum  $j=3/2$ .  $j$ - $j$  coupling between two holes in  $A^0X$  results in the two-hole states with the net angular momentum  $J=0$  or  $J=2$ . Interaction with the tetrahedral impurity potential and coupling to the electron can further split the two-hole state  $J=2$ .

The early studies<sup>4-7</sup> of  $A^0X$  in Si demonstrated that for Al, Ga, and In the energy of the two-hole state  $J=0$  is significantly lower (by approximately 1.2 meV for Al, 1.6 meV for Ga, and  $\approx 3$  meV for In) than the energy of the  $J=2$  state. This ordering of the two-hole states contradicts Hund's rule,<sup>8</sup> which predicts that the state with maximum  $J$  must have the lowest energy. Ham and Leung<sup>9</sup> recently explained this inverted ordering of the two-hole states in  $A^0X$  as arising from a Jahn-Teller effect<sup>10</sup> (JTE). In  $A^0X$  on Al, Ga, and In, only the  $J=0$  two-hole state is populated at liquid-He temperatures. The state  $J=0$  is a singlet, and no interaction can split it. The only remaining degeneracy is that of the electron

states arising from the sixfold degeneracy of the conduction-band minimum. However, interaction with the impurity center can lift this sixfold degeneracy. As a result, the electron states involving different combinations of the six conduction-band minima, referred to as the valley-orbit (VO) states, can have different energies. The size of the splitting between the VO states, the valley-orbit splitting (VOS), depends on the potential in the immediate vicinity of the impurity ion, the central cell potential (CCP). Since the negatively charged acceptor ion  $A^-$  repels the electron in  $A^0X$ , the electron interacts with the CCP rather weakly. Therefore, the VOS in  $A^0X$  is very small, and it was neglected in the early studies.<sup>11</sup> Accurate measurement of the VOS and identification of the VO states in  $A^0X$  bound to different  $A^0$  species may be of significant interest, since it provides additional information on the CCP's of these acceptors and the  $A^0X$  wave functions. This study provides the most comprehensive description of the  $A^0X$  ground state and transitions available for any indirect-gap semiconductor.

The first experimental evidence of VOS in  $A^0X$  was reported by Elliot *et al.*<sup>7</sup> who observed a doublet structure for the  $J=0$  component in the near infrared (NIR) absorption spectra of  $Al^0X$ . Later, Karasyuk and Pokrovskii<sup>12</sup> measured the size of VOS in  $B^0X$  using a scanning Fabry-Pérot interferometer to resolve the fine structure in the PL spectra of Si(B) under uniaxial stress. Gorbunov, Kaminskii, and Safonov<sup>13</sup> observed all three VO states of  $Al^0X$  and determined the ordering of the VO states in  $Al^0X$  and  $Ga^0X$  using PL spectroscopy under uniaxial stress with a resolution of 0.045 meV for Al and 0.012 meV for Ga. The constant en-

ergy surfaces in the vicinity of the Si conduction-band minima are strongly anisotropic and elongated along the  $\langle 001 \rangle$  directions. Karasyuk, Brake, and Thewalt<sup>14</sup> found recently that this anisotropy causes additional splitting of the  $A^0X$  VO states in strong magnetic fields, due to the differences in quadratic diamagnetic shifts. The pattern of this diamagnetic VOS allows unambiguous identification of the  $A^0X$  VO states.

At zero field, the electron in  $A^0X$  can occupy one of the three VO states with the single-electron wave functions transforming according to the irreducible representations  $\Gamma_1$ ,  $\Gamma_3$ , and  $\Gamma_5$  (notation of Koster *et al.*<sup>15</sup>) of the point group  $T_d$  that describes the symmetry of a substitutional site in the Si lattice.<sup>11</sup> The state  $\Gamma_1$  is a singlet,  $\Gamma_3$  is a doublet, and  $\Gamma_5$  is a triplet. A  $J=0$   $A^0X$  has only three energy levels corresponding to the three valley-orbit states of the electron. The final state for the principal optical transitions observed in PL spectra of  $A^0X$  is the ground state of the neutral acceptor  $A^0$ . Theoretical treatments of shallow acceptors are usually based on the effective-mass approximation<sup>16</sup> (EMA), predicting a single energy level for the ground state of  $A^0$  well separated from the rest of the spectrum. Three initial-state levels and a single final-state level produce no more than three spectral components. However, Thewalt and Brake<sup>17</sup> recently resolved more than three spectral components in PL spectra of  $Al^0X$ ,  $Ga^0X$ , and  $In^0X$  using a high-resolution Fourier-transform interferometer. At liquid-He temperatures, when only the  $J=0$  state of  $A^0X$  is populated, they observed six well-resolved components for Al, five for Ga, and four for In. Further investigations<sup>18,19</sup> confirmed that this fine structure is sample independent (provided that inhomogeneous line broadening does not exceed the size of the splittings). For Tl, the  $A^0X$  PL spectra recorded recently at liquid-He temperatures by Karasyuk and An<sup>20</sup> contain three components that are much narrower than the four components observed previously<sup>21</sup> at temperatures above 15 K.

Karasyuk *et al.*<sup>18,19</sup> demonstrated recently that the additional fine structure in  $Al^0X$ ,  $Ga^0X$ , and  $In^0X$  spectra is due to an intrinsic splitting of the  $A^0$  ground state whose origin has not been elucidated decisively yet, but which may be due to the JTE. The Zeeman effect can provide additional information that may help to determine the mechanism of this splitting. The  $In^0$  ground-state splitting is more difficult to observe than that of  $Al^0$  and  $Ga^0$ ; and does not result in resolved splittings of  $In^0X$  PL.<sup>18,19</sup> All four peaks observed in  $In^0X$  PL are due to the fourfold splitting of the  $In^0X$  states. In the present work, we demonstrate on the basis of Zeeman effect measurements that spin-orbit coupling is responsible for an additional splitting of the  $\Gamma_5$  VO state of  $In^0X$ .

A detailed high-resolution investigation of the Zeeman effect on  $B^0X$  was reported recently by Karasyuk, Brake, and Thewalt.<sup>14</sup> For the other group-III acceptors in Si, only three previous PL studies dealt with the Zeeman effect including a recent work by Karasyuk and An<sup>20</sup> on Si(Tl). Kulakovskii and Malyavkin<sup>22</sup> studied PL spectra of  $Al^0X$  in magnetic fields of up to 8 T with 0.1-meV resolution. They confirmed that the ground two-hole state is a singlet and determined that the states with  $J=2$  are not populated in this range of fields at 1.8 K. Weber, Conzelman, and Sauer<sup>23</sup> studied the Zeeman effect on  $A^0X$  for all group-III acceptors in magnetic fields of up to 5.3 T using a grating spectrometer with

$\sim 0.07$ -meV resolution. They resolved four components in the Zeeman spectra for B, Al, and Ga, three for In, and five for Tl. Only the Tl spectra were polarization dependent. In both studies the spectra showed no trace of the VOS, and terms quadratic in magnetic field were not included in the analysis.

In the present work, we investigate the Zeeman effect on  $A^0X$  in silicon doped with Al, Ga, In, and Tl using a BOMEM DA8 Fourier-transform spectrometer and magnetic fields up to 14.5 T. The very high resolution of 0.0025 meV allowed us to resolve up to 30 components in the spectra, to observe the diamagnetic VOS, and to measure  $g$  factors with significantly better accuracy than in the previous studies, as well as quadratic diamagnetic shift constants. All experimental results can be explained on the basis of the shell model<sup>11</sup> of  $A^0X$ . We describe the VOS in magnetic fields following the theoretical treatment of  $B^0X$  by Karasyuk, Brake, and Thewalt,<sup>14</sup> and use expressions for the energy levels of  $A^0$  from the paper by Bhattacharjee and Rodrigues.<sup>24</sup> We have also calculated the selection rules for optical transitions from different VO states of  $A^0X$  in magnetic fields with [001], [111], and [110] orientations. The selection rules for the [001] field were obtained previously by Gorbunov, Kaminiskii, and Safonov<sup>13</sup> in a different basis. We determined the parameters of the selection rules from the amplitude ratios in the zero-field PL spectra and used them to simulate the spectra in magnetic fields.

## II. THEORY

### A. $A^0$ in magnetic fields

Bhattacharjee and Rodrigues<sup>24</sup> provided a detailed group theoretical analysis of the Zeeman effect on acceptors in Si and Ge (not taking into account the intrinsic splitting of the ground state discovered recently<sup>18,19</sup>). The intrinsic splitting is small (0.014 meV for  $Al^0$  and  $Ga^0$ , and 0.019 meV for  $In^0$ ) in comparison with the Zeeman splittings in magnetic fields above 1T. At lower fields it may produce considerable deviations from the theory, but the multitude of overlapping components in the spectra at low fields hinders the data analysis in this region in any case. For simplicity, we shall neglect the intrinsic splitting of the  $A^0$  ground state and describe it in a usual way as a quadruplet represented by the set of four wave functions:<sup>24</sup>

$$\begin{aligned}\psi_{+3/2} &= \frac{1}{\sqrt{2}} (X + iY)|\alpha\rangle, \\ \psi_{+1/2} &= \frac{i}{\sqrt{6}} [(X + iY)|\beta\rangle - 2Z|\alpha\rangle], \\ \psi_{-1/2} &= \frac{1}{\sqrt{6}} [(X - iY)|\alpha\rangle + 2Z|\beta\rangle], \\ \psi_{-3/2} &= \frac{i}{\sqrt{2}} (X - iY)|\beta\rangle,\end{aligned}\tag{1}$$

forming the basis of the irreducible representation  $\Gamma_8$ . Here,  $X$ ,  $Y$ , and  $Z$  denote the functions of spatial coordinates  $x, y, z$

transforming as  $yz$ ,  $zx$ , and  $xy$ ,  $|\alpha\rangle$  and  $|\beta\rangle$  are the  $s=\frac{1}{2}$  spinors with the spin projections  $m_s=+\frac{1}{2}$  and  $-\frac{1}{2}$ , and the functions (1) are labeled by the subscripts according to the angular momentum projections on the  $[001]$  axis  $m_j=+\frac{3}{2}$ ,  $+\frac{1}{2}$ ,  $-\frac{1}{2}$ ,  $-\frac{3}{2}$ .

The effect of a uniform magnetic field  $\mathbf{B}$  with Cartesian components  $(B_x, B_y, B_z)$  with respect to the crystal cubic axes on the ground acceptor level  $\Gamma_8$  can be accounted for by the Hamiltonian matrix<sup>24</sup>

$$H^{(8)}(\mathbf{B}) = \mu_B g_1 (\mathbf{B} \cdot \mathbf{J}) + \mu_B g_2 (B_x J_x^3 + B_y J_y^3 + B_z J_z^3) + q_1 B^2 + q_2 (\mathbf{B} \cdot \mathbf{J})^2 + q_3 (B_x^2 J_x^2 + B_y^2 J_y^2 + B_z^2 J_z^2) \quad (2)$$

where  $\mu_B$  is the Bohr magneton,  $g_1$  and  $g_2$  are the  $g$  factors,  $q_1$ ,  $q_2$ , and  $q_3$  are the diamagnetic shift constants, and  $\mathbf{J}=(J_x, J_y, J_z)$  represents the angular momentum matrices in the basis (1):

$$J_x = \frac{i}{2} \begin{bmatrix} 0 & \sqrt{3} & 0 & 0 \\ -\sqrt{3} & 0 & 2 & 0 \\ 0 & -2 & 0 & \sqrt{3} \\ 0 & 0 & -\sqrt{3} & 0 \end{bmatrix},$$

$$J_y = \frac{1}{2} \begin{bmatrix} 0 & \sqrt{3} & 0 & 0 \\ \sqrt{3} & 0 & 2 & 0 \\ 0 & 2 & 0 & \sqrt{3} \\ 0 & 0 & \sqrt{3} & 0 \end{bmatrix},$$

$$J_z = \frac{1}{2} \begin{bmatrix} 3 & 0 & 0 & 0 \\ 0 & 1 & 0 & 0 \\ 0 & 0 & -1 & 0 \\ 0 & 0 & 0 & -3 \end{bmatrix}. \quad (3)$$

The  $A^0$  energy levels in magnetic field  $\mathbf{B}$  can be obtained by diagonalization of the Hamiltonian matrix (2). When  $\mathbf{B}$  is oriented along one of the three main crystallographic directions  $\langle 001 \rangle$ ,  $\langle 111 \rangle$ , or  $\langle 110 \rangle$ , solutions can be expressed in a simple analytical form furnished by Bhattacharjee and Rodrigues.<sup>24</sup>

### B. $A^0X$ in magnetic fields

$A^0X$  with holes in the  $J=0$  state can be represented by a product of a single-electron function  $\psi_e$  and the two-hole function  $\Psi_{hh}$  that transforms according to the unit representation  $\Gamma_1$  of  $T_d$ . We assume that magnetic fields do not mix the two-hole state  $\Gamma_1$  with the other two-hole states, which have much higher energy. In this case, the effect of magnetic field on the holes in  $A^0X$  amounts to the diamagnetic shift  $E_{hh}^{\text{dia}}(\mathbf{B}) = q_0^{hh} B^2$  that can be added to the single-electron energy levels in order to obtain the energy levels of  $A^0X$ .

The electron wave function  $\psi_e$  in  $A^0X$  is similar to the wave function of a shallow neutral donor. It can be represented by a product of a spatial part  $\phi(\mathbf{r}_e)$  and a spinor with the spin  $s=\frac{1}{2}$  when the spin-orbit coupling can be neglected. The spatial part  $\phi(\mathbf{r}_e)$  can be decomposed into a linear combination<sup>16</sup>

$$\phi^{(n)} = \sum_{m=1}^6 \alpha_m^{(n)} F_m \varphi_m \quad (4)$$

of the Bloch functions  $\varphi_m$  in the six conduction-band minima of Si multiplied by the smooth envelope functions  $F_m$ . Six such linear combinations  $\phi^{(n)}$  form the bases of the irreducible representations  $\Gamma_1$ ,  $\Gamma_3$ , and  $\Gamma_5$  of  $T_d$ :

$$\phi^{(1)}: \alpha_m^{(1)} = \frac{1}{\sqrt{6}} (111111) \quad (\Gamma_1), \quad (5)$$

$$\phi^{(31)}: \alpha_m^{(31)} = \frac{1}{2\sqrt{3}} (\overline{1111}22) \quad (\Gamma_3), \quad (6)$$

$$\phi^{(32)}: \alpha_m^{(32)} = \frac{1}{2} (111\overline{1}00)$$

$$\phi^{(5x)}: \alpha_m^{(5x)} = \frac{1}{\sqrt{2}} (1\overline{1}0000)$$

$$\phi^{(5y)}: \alpha_m^{(5y)} = \frac{1}{\sqrt{2}} (001\overline{1}00) \quad (\Gamma_5). \quad (7)$$

$$\phi^{(5z)}: \alpha_m^{(5z)} = \frac{1}{\sqrt{2}} (00001\overline{1})$$

In this notation,  $\alpha_m$  is equal to the  $m$ th number enclosed in parentheses divided by the common denominator shown in front of the parentheses. Negative coefficients have a bar over the top. The 12 products

$$\phi^{(n)}|\alpha\rangle, \phi^{(n)}|\beta\rangle, \quad n=1, \dots, 6 \quad (8)$$

of the functions (5)–(7) and the spinors  $|\alpha\rangle$  and  $|\beta\rangle$  form the complete set of the zeroth-order eigenfunctions for the electron in  $A^0X$ .

The VOS Hamiltonian matrix in the basis (8) has the form

$$H_e^{\text{VOS}} = \begin{bmatrix} \Delta_{15}^{\text{VO}} & 0 & 0 & 0 & 0 & 0 \\ 0 & \Delta_{35}^{\text{VO}} & 0 & 0 & 0 & 0 \\ 0 & 0 & \Delta_{35}^{\text{VO}} & 0 & 0 & 0 \\ 0 & 0 & 0 & 0 & 0 & 0 \\ 0 & 0 & 0 & 0 & 0 & 0 \\ 0 & 0 & 0 & 0 & 0 & 0 \end{bmatrix} \otimes I_s, \quad (9)$$

where  $I_s$  is a  $2 \times 2$  unit matrix in the basis of the spinors  $|\alpha\rangle$  and  $|\beta\rangle$ . The constants  $\Delta_{15}^{\text{VO}}$  and  $\Delta_{35}^{\text{VO}}$  determine the zero-field VOS of the states  $\Gamma_1$  and  $\Gamma_3$ , respectively, relative to the state  $\Gamma_5$ .

If  $\phi^{(n)}$  includes only one conduction-band minimum ( $\alpha_m^{(n)} = \delta_m^n$ ), interaction with magnetic field  $\mathbf{B}$  can be accounted for by the Hamiltonian<sup>14</sup>

$$H_e(\mathbf{B}) = \mu_B g_e (B_x S_x + B_y S_y + B_z S_z) + q_{\parallel}^e B^2 \cos^2 \beta + q_{\perp}^e B^2 \sin^2 \beta, \quad (10)$$

where  $g_e$  is the electron  $g$  factor,  $q_{\parallel}^e$  and  $q_{\perp}^e$  are the diamagnetic shift constants,  $\beta$  is the angle between  $\mathbf{B}$  and the corresponding conduction-band valley, and

$$S_x = \frac{1}{2} \begin{bmatrix} 0 & 1 \\ 1 & 0 \end{bmatrix}, \quad S_y = \frac{1}{2} \begin{bmatrix} 0 & -i \\ i & 0 \end{bmatrix}, \quad S_z = \frac{1}{2} \begin{bmatrix} 1 & 0 \\ 0 & -1 \end{bmatrix} \quad (11)$$

are the spin matrices. Effective-mass anisotropy in the conduction-band minima accounts for the difference in quadratic diamagnetic shifts for the valleys parallel ( $q_{\parallel}^e$ ) and perpendicular ( $q_{\perp}^e$ ) to the magnetic field. The corresponding Hamiltonian matrix in the basis (8) for  $\mathbf{B}$  lying in the (110) plane has the form

$$H_e(\mathbf{B}) = I_{\text{VO}} \otimes \mu_B g_e (\mathbf{B} \cdot \mathbf{S}) + q_0^e B^2 I_{\text{VO}} \otimes I_s + \frac{1}{6} q_d^e B^2 (2 \cos^2 \theta - \sin^2 \theta) \times \begin{bmatrix} 0 & \sqrt{2} & 0 & 0 & 0 & 0 \\ \sqrt{2} & 1 & 0 & 0 & 0 & 0 \\ 0 & 0 & -1 & 0 & 0 & 0 \\ 0 & 0 & 0 & -1 & 0 & 0 \\ 0 & 0 & 0 & 0 & -1 & 0 \\ 0 & 0 & 0 & 0 & 0 & 2 \end{bmatrix} \otimes I_s, \quad (12)$$

where  $I_{\text{VO}}$  is the  $6 \times 6$  unit matrix,  $\theta$  is the angle between  $\mathbf{B}$  and the [001] axis,  $q_0^e \equiv \frac{1}{3} q_{\parallel}^e + \frac{2}{3} q_{\perp}^e$ , and  $q_d^e \equiv q_{\parallel}^e - q_{\perp}^e$ .

The first two terms in  $H_e(\mathbf{B})$  determine the isotropic paramagnetic splitting of the electron energy levels  $E_e^{\text{para}} = g_e \mu_B B m_s$ ,  $m_s = \pm \frac{1}{2}$ , and the isotropic diamagnetic shift  $E_{e0}^{\text{dia}} = q_0^e B^2$  that are the same for all the valley-orbit states. Only the last term in  $H_e(\mathbf{B})$  depends on the VO state. This term disappears when  $\mathbf{B}$  is parallel to the  $\langle 111 \rangle$  direction and all the valleys form the same angle with  $\mathbf{B}$  ( $\cos^2 \theta = 1/3$ ). The  $A^0X$  energy levels can be found by diagonalization of the net Hamiltonian matrix  $H_{A^0X}(\mathbf{B}) = H^{\text{VOS}} + H_e(\mathbf{B}) + E_{hh}^{\text{dia}}(\mathbf{B})$ . Magnetic fields with any orientation other than  $\langle 111 \rangle$  produce additional VOS and mix the state  $\phi^{(1)}$  with the  $\Gamma_3$  state  $\phi^{(31)}$  resulting in the limit of infinite  $B$  in the VO states:

$$\phi^{(1x)}: \quad \alpha_m^{(1x)} = \frac{1}{2} (111100), \quad (13)$$

$$\phi^{(1z)}: \quad \alpha_m^{(1z)} = \frac{1}{\sqrt{2}} (000011). \quad (14)$$

In the absence of the spin-orbit coupling, the  $A^0X$  energy levels for magnetic fields lying in the (110) plane can be obtained in a simple analytical form:

$$E_{1\pm} = E_0 \pm \frac{1}{2} g_e \mu_B B + q_0 B^2 + \Delta_{15}^{\text{VO}} + \frac{1}{2} \left\{ \Delta_{31}^{\text{VO}} + b + 3b \left[ 1 + \frac{2}{9} \frac{\Delta_{31}^{\text{VO}}}{b} + \left( \frac{\Delta_{31}^{\text{VO}}}{3b} \right)^2 \right]^{1/2} \right\}, \quad (15)$$

$$E_{2\pm} = E_0 \pm \frac{1}{2} g_e \mu_B B + q_0 B^2 + \Delta_{15}^{\text{VO}} + \frac{1}{2} \left\{ \Delta_{31}^{\text{VO}} + b - 3b \left[ 1 + \frac{2}{9} \frac{\Delta_{31}^{\text{VO}}}{b} + \left( \frac{\Delta_{31}^{\text{VO}}}{3b} \right)^2 \right]^{1/2} \right\}, \quad (16)$$

$$E_{3\pm} = E_0 \pm \frac{1}{2} g_e \mu_B B + q_0 B^2 + \Delta_{35}^{\text{VO}} - b, \quad (17)$$

$$E_{4\pm} = E_{5\pm} = E_0 \pm \frac{1}{2} g_e \mu_B B + q_0 B^2 - b, \quad (18)$$

$$E_{6\pm} = E_0 \pm \frac{1}{2} g_e \mu_B B + q_0 B^2 + 2b, \quad (19)$$

$$\Delta_{31}^{\text{VO}} \equiv \Delta_{35}^{\text{VO}} - \Delta_{15}^{\text{VO}}, \quad b \equiv \frac{1}{6} q_d^e B^2 (2 \cos^2 \theta - \sin^2 \theta),$$

where  $E_0$  is the zero-field  $\Gamma_5$  energy level, the  $\pm$  terms correspond to  $m_s = +\frac{1}{2}$ , and  $m_s = -\frac{1}{2}$ .

### C. The effects of spin-orbit coupling

Near-infrared absorption studies of shallow donors in Si showed that spin-orbit coupling (SOC) can split the  $1s(\Gamma_5)$  donor states, although this splitting is much smaller than the VOS.<sup>25</sup> SOC cannot split the  $\Gamma_1$  [Eq. (5)] or the  $\Gamma_3$  [Eq. (6)] VO states since the direct products  $\Gamma_1 \otimes \Gamma_6 = \Gamma_6$  and  $\Gamma_3 \otimes \Gamma_6 = \Gamma_8$  transform according to the irreducible representations of  $T_d$ . On the other hand, SOC can split the  $\Gamma_5$  states (7) into a Kramers doublet  $\Gamma_7$  and a quadruplet  $\Gamma_8$  since  $\Gamma_5 \otimes \Gamma_6 = \Gamma_7 + \Gamma_8$ . In principle, SOC can cause mixing of the VO states  $\Gamma_3$  and  $\Gamma_5$ ,<sup>26</sup> but we assume that the VOS between these states is large enough and neglect the effect of SOC on the VO states  $\Gamma_3$ . For the states  $\Gamma_5$ , SOC can be accounted for in this case by the Hamiltonian<sup>25</sup>

$$H_e^{\text{SO}} = \lambda^{\text{SO}} (I_x \otimes S_x + I_y \otimes S_y + I_z \otimes S_z), \quad (20)$$

where  $\lambda^{\text{SO}}$  is the spin-orbit interaction constant and

$$I_x = \begin{bmatrix} 0 & 0 & 0 \\ 0 & 0 & -i \\ 0 & i & 0 \end{bmatrix}, \quad I_y = \begin{bmatrix} 0 & 0 & i \\ 0 & 0 & 0 \\ -i & 0 & 0 \end{bmatrix}, \quad I_z = \begin{bmatrix} 0 & -i & 0 \\ i & 0 & 0 \\ 0 & 0 & 0 \end{bmatrix} \quad (21)$$

are the angular momentum matrices in the basis of the  $\Gamma_5$  VO functions (7) corresponding to the orbital angular momentum  $l=1$ . The zero-field splitting between the  $\Gamma_7$  and  $\Gamma_8$  sublevels is equal to  $\frac{3}{2} \lambda^{\text{SO}}$ . The quadruplet  $\Gamma_8$  has higher energy than the doublet  $\Gamma_7$  when  $\lambda^{\text{SO}} > 0$ .

SOC can cause additional splitting of the  $\Gamma_5$  energy levels in magnetic fields. Since the SOC is rather weak, all the electron states have almost definite spin projections on the field direction above 1 T. Three linear combinations of the functions (7) with angular momentum projections  $m_l$  correspond to the single-electron eigenfunctions in strong [001] and [111] magnetic fields:

$$\phi_{[001]}^{(5+)} = \frac{1}{\sqrt{2}} (\phi^{(5x)} + i \phi^{(5y)}), \quad m_l = +1, \quad \phi_{[001]}^{(5-)} = \frac{1}{\sqrt{2}} (\phi^{(5x)} - i \phi^{(5y)}), \quad m_l = -1, \quad (22)$$

$$\phi_{[001]}^{(50)} = \phi^{(5z)}, \quad m_l = 0$$

for  $\mathbf{B} \parallel [001]$ , and

$$\phi_{[111]}^{(5+)} = \frac{1}{2\sqrt{3}} [(1 - i\sqrt{3})\phi^{(5x)} + (1 + i\sqrt{3})\phi^{(5y)} - 2\phi^{(5z)}],$$

$$m_l = +1,$$

$$\phi_{[111]}^{(5-)} = \frac{1}{2\sqrt{3}} [(1 + i\sqrt{3})\phi^{(5x)} + (1 - i\sqrt{3})\phi^{(5y)} - 2\phi^{(5z)}],$$

$$m_l = -1, \quad (23)$$

$$\phi_{[111]}^{(50)} = \frac{1}{\sqrt{3}} [\phi^{(5x)} + \phi^{(5y)} + \phi^{(5z)}], \quad m_l = 0$$

for  $\mathbf{B} \parallel [111]$ .

The corresponding  $\Gamma_5$  energy levels are

$$E_{4\pm} = E_0 \pm \frac{1}{2} g_e \mu_B B + q_0 B^2 - b \pm \frac{\lambda^{\text{SO}}}{2} \quad \text{for } \phi^{(5+)}, \quad (24)$$

$$E_{5\pm} = E_0 \pm \frac{1}{2} g_e \mu_B B + q_0 B^2 - b \mp \frac{\lambda^{\text{SO}}}{2} \quad \text{for } \phi^{(5-)}, \quad (25)$$

$$E_{6\pm} = E_0 \pm \frac{1}{2} g_e \mu_B B + q_0 B^2 + 2b \quad \text{for } \phi^{(50)} \quad (26)$$

instead of those given by Eqs. (18) and (19).

The proper VO combinations change significantly in a wide range of [110] magnetic fields due to the interplay between the anisotropic diamagnetic shifts and SOC. Equations (18) and (19) give the values of the  $\Gamma_5$  energy levels in strong [110] fields when  $q_d B^2 \gg \lambda^{\text{SO}}$ . The corresponding VO combinations can be chosen as

$$\phi_{[110]}^{(5y'')} = \frac{1}{\sqrt{2}} (-\phi^{(5x)} + \phi^{(5y)}), \quad (27)$$

$$\phi_{[110]}^{(5z'')} = \frac{1}{\sqrt{2}} (\phi^{(5x)} + \phi^{(5y)})$$

for the level (18), and

$$\phi_{[110]}^{(5x'')} = -\phi^{(5z)} \quad (28)$$

for the level (19). In the range of  $B$  where  $\lambda^{\text{SO}}$  is comparable with  $q_d B^2$ , but still  $\lambda^{\text{SO}} \ll g_e \mu_B B$ , the electron energy levels can be evaluated according to the formula

$$\begin{aligned} E_{4\pm} &= E_0 \pm \frac{1}{2} g_e \mu_B B + q_0 B^2 - \frac{1}{12} q_d B^2 + \frac{1}{4} q_d B^2 \gamma \\ &\approx E_0 \pm \frac{1}{2} g_e \mu_B B + q_0 B^2 + \frac{1}{6} q_d B^2 + \frac{\lambda^{\text{SO}}}{2} \rho, \\ \rho &\equiv \frac{\lambda^{\text{SO}}}{q_d B^2}, \quad \gamma = \sqrt{1 + 4\rho^2} \end{aligned} \quad (29)$$

for the eigenfunctions

$$\psi_{+[110]}^{(5+)} = \frac{1}{\sqrt{2\gamma(\gamma+1)}} [-i\rho\phi_{[110]}^{(5x'')} + (1+\gamma)\phi_{[110]}^{(5y'')}] \alpha''_{[110]} \quad (30)$$

and

$$\psi_{-[110]}^{(5+)} = \frac{1}{\sqrt{2\gamma(\gamma+1)}} [i\rho\phi_{[110]}^{(5x'')} + (1+\gamma)\phi_{[110]}^{(5y'')}] \beta''_{[110]}, \quad (31)$$

$$\begin{aligned} E_{5\pm} &= E_0 \pm \frac{1}{2} g_e \mu_B B + q_0 B^2 - \frac{1}{12} q_d B^2 - \frac{1}{4} q_d B^2 \gamma \\ &\approx E_0 \pm \frac{1}{2} g_e \mu_B B + q_0 B^2 - \frac{1}{3} q_d B^2 - \frac{\lambda^{\text{SO}}}{2} \rho \end{aligned} \quad (32)$$

for the eigenfunctions

$$\psi_{+[110]}^{(5-)} = \frac{1}{\sqrt{2\gamma(\gamma+1)}} [(1+\gamma)\phi_{[110]}^{(5x'')} - i\rho\phi_{[110]}^{(5y'')}] \alpha''_{[110]}, \quad (33)$$

and

$$\psi_{-[110]}^{(5-)} = \frac{1}{\sqrt{2\gamma(\gamma+1)}} [(1+\gamma)\phi_{[110]}^{(5x'')} + i\rho\phi_{[110]}^{(5y'')}] \beta''_{[110]}, \quad (34)$$

$$E_{6\pm} = E_0 \pm \frac{1}{2} g_e \mu_B B + q_0 B^2 + \frac{1}{6} q_d B^2 \quad (35)$$

for

$$\psi_{+[110]}^{(50)} = \phi_{[110]}^{(5z'')} \alpha''_{[110]} \quad \text{and} \quad \psi_{-[110]}^{(50)} = \phi_{[110]}^{(5z'')} \beta''_{[110]}, \quad (36)$$

where

$$\alpha''_{[110]} = \frac{1}{\sqrt{2}} (\omega|\alpha\rangle + \omega^*|\beta\rangle),$$

$$\beta''_{[110]} = \frac{1}{\sqrt{2}} (-\omega|\alpha\rangle + \omega^*|\beta\rangle), \quad \omega \equiv e^{-i(\pi/8)} \quad (37)$$

are the spinors with the spin projections  $m_s = \pm \frac{1}{2}$  on the [110] quantization axis.<sup>24</sup>

Figure 1 shows the evolution of the VOS in  $\langle 001 \rangle$ ,  $\langle 111 \rangle$ , and  $\langle 110 \rangle$  magnetic fields. Without SOC [Figs. 1(a), 1(b), and 1(c)] the three VO states  $\Gamma_1$ ,  $\Gamma_3$ , and  $\Gamma_5$  remain unchanged in  $\langle 111 \rangle$  magnetic fields, and split into five energy levels in  $\langle 001 \rangle$  and  $\langle 110 \rangle$  magnetic fields. The levels  $5x(5y)$ ,  $5z$ , and  $3z$  shift linearly with  $B^2$ . The levels  $1x$  and  $1z$  shift nonlinearly with  $B^2$  due to mixing of the  $\Gamma_1$  and the  $\Gamma_3$  VO states. SOC [Figs. 1(d), 1(e), and 1(f)] affects only the  $\Gamma_5$  VO states. It splits them into the doublet  $\Gamma_7(\Gamma_5)$  and the quadruplet  $\Gamma_8(\Gamma_5)$  at zero field. Magnetic fields split the  $\Gamma_5$  VO states further into three energy levels. Two of these levels  $5y''$  and  $5z''$  merge in strong  $\langle 110 \rangle$  fields.

#### D. Selection rules

The Tables I, II, and III list the selection rules that govern the relative probabilities of optical transitions in magnetic fields from  $A^0X$  with a certain VO state and  $m_s = \pm \frac{1}{2}$  to the  $A^0$  states with  $m_j = \pm \frac{3}{2}, \pm \frac{1}{2}$ . The oscillator strengths of these transitions are proportional to the square of the modulus of the electric dipole matrix elements listed in the tables expressed in terms of three independent constants  $\gamma$ ,  $\lambda$ , and  $\eta$ . The Appendix contains the details of calculations of the selection rules. The relative intensities of different spectral components depend on the two ratios,  $\gamma/\eta$  and  $\lambda/\eta$ . Assuming equal population of the  $\Gamma_1$ ,  $\Gamma_3$ , and  $\Gamma_5 A^0X$  energy levels at zero field, the relative intensities of the corresponding PL components should be in a ratio  $(2\eta + \lambda)^2 : 2(\eta - \lambda)^2 : 6\gamma^2$ .<sup>27</sup> We

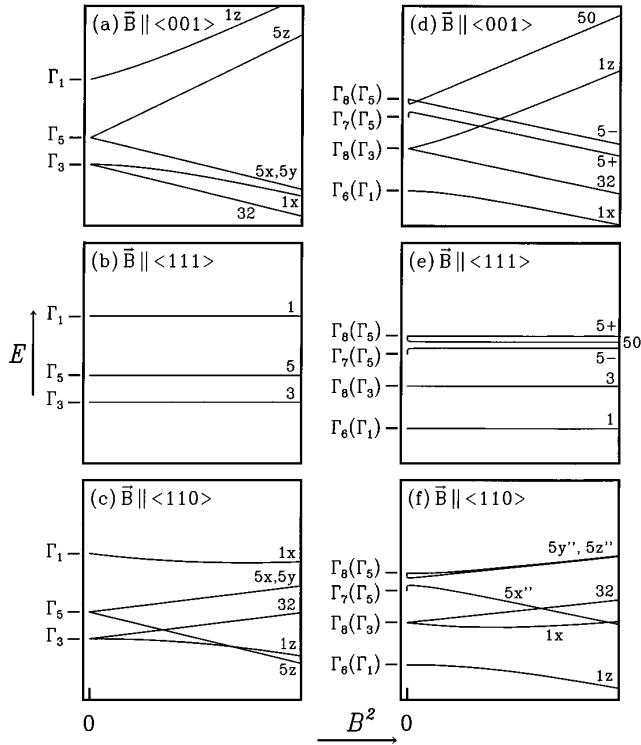


FIG. 1. Valley-orbit splitting (VOS) of the acceptor bound exciton ( $A^0X$ ) energy levels as a function of the square of the magnetic field  $B$ . (a),(d)  $\langle 001 \rangle$ , (b),(e)  $\langle 111 \rangle$ , and (c),(f)  $\langle 110 \rangle$ , sample orientations. Horizontal marks show the  $A^0X$  energy levels at  $B=0$  with (d)–(f) and without (a)–(c) spin-orbit coupling (SOC) labeled by the corresponding irreducible representations of the point group  $T_d$ . The ordering of the valley-orbit (VO) states in (a)–(c) corresponds to that of  $Al^0X$  or  $Ga^0X$ , while (d)–(f) corresponds to that of  $In^0X$ . The energy levels in strong magnetic fields are labeled on the right-hand side by the superscripts of the corresponding eigenfunctions [see Eqs. (5)–(7), (13), (14), (22), (23), (27), and (28) in the text].

have determined the ratios  $\gamma/\eta$  and  $\lambda/\eta$  by fitting to the amplitude ratios in the zero-field spectra, and then used them for calculation of the theoretical spectra in magnetic fields.

### III. EXPERIMENT

#### A. Experimental techniques

The float zone silicon samples doped with Al, Ga, In, and Tl in concentrations from  $10^{14}$  to  $2 \times 10^{15} \text{ cm}^{-3}$  were cut in the shape of  $2 \times 2 \times 20\text{-mm}^3$  parallelepipeds with long sides x-ray oriented along the  $\langle 111 \rangle$ ,  $\langle 110 \rangle$ , or  $\langle 001 \rangle$  crystallographic directions. The samples were immersed in a liquid-He bath within the 2-in. bore of a 15-T Oxford Instruments superconducting solenoid. The sample's long axis was oriented along the magnetic field. A  $45^\circ$  mirror located near the sample reflected a 0.5-W cw  $0.98\text{-}\mu\text{m}$  Ti:sapphire excitation laser beam towards the sample, and the luminescence radiation from the sample towards the axial exit window of the cryostat. A 6-in. fused silica lens collimated the luminescence beam from the sample into a BOMEM DA8 Michelson interferometer. A 77-K Ge photodetector (North Coast)

was used to record PL interferograms, which afterwards were Fourier transformed into PL spectra with resolution of up to  $0.0025 \text{ meV}$ .

#### B. Zero-field PL spectra

In zero magnetic field and at temperatures of  $\sim 2 \text{ K}$ , we resolved in the no-phonon (NP) spectra of the  $A^0X$  six components for  $Al^0X$ , five for  $Ga^0X$ , four components for  $In^0X$ , and three for  $Tl^0X$  (Figs. 2 and 3). In Fig. 2, the zero-field  $Al^0X$  and  $Ga^0X$  spectra can be decomposed into the sum of three doublets having identical line shapes for each  $A^0X$ , as shown in the insets on the right-hand side. The triplet structure arises from the  $\Gamma_1$ ,  $\Gamma_3$ , and  $\Gamma_5$  VO states of  $A^0X$ , while the doublets arise from the  $A^0$  ground-state splitting, as previously demonstrated by temperature-dependent PL, absorption, and excitation spectroscopy.<sup>18,19</sup> As described above, the  $In^0X$  has four states due to the SOC splitting of the  $\Gamma_5$  VO state. While the doublet structure shown on the right-hand side of Fig. 2 for the  $In^0X$  spectrum is not immediately evident in the PL spectrum, it is required to obtain a good fit, and is more evident in temperature-dependent absorption spectra.<sup>19</sup> The vertical bars indicate the positions and the relative amplitudes of the low-energy peaks in the doublets. All three VO states can be observed in the spectra of  $Tl^0X$ , Fig. 3, although here the states  $\Gamma_3$  and  $\Gamma_5$  have 1.2 and 1.3 meV higher energy than the state  $\Gamma_1$ , and no extra doublet structure due to splitting of  $Tl^0$  has been resolved. The  $Tl^0X$  lifetime must be too short for complete thermal equilibrium between the VO states to be reached. The origin of the small  $A^0$  splitting has yet to be conclusively determined, and we have ignored it in the analysis of the Zeeman effect.

#### C. PL spectra in magnetic fields

Figures 4–8 show the spectra of  $Al^0X$ ,  $In^0X$ , and  $Tl^0X$  in magnetic fields. The Zeeman spectra of  $Ga^0X$  are very similar to those of  $Al^0X$  except for the small differences in the VOS and we do not show them for the sake of brevity. The Zeeman spectra contain a large number of well-resolved, narrow (full width at half maximum of  $\approx 0.01 \text{ meV}$  for Al and Ga,  $\approx 0.015 \text{ meV}$  for In, and  $\approx 0.05 \text{ meV}$  for Tl) components. Each component corresponds to an optical transition from a particular VO state (Fig. 1) of  $A^0X$  with spin projections on the magnetic field  $m_s = \pm \frac{1}{2}$  to one of the  $A^0$  sublevels with angular momentum projections  $m_j = \pm 3/2, \pm 1/2$  (Fig. 9). Transitions with  $|m_j - m_s| > 1$  are prohibited.

In the case of Al and Ga the amplitudes of the PL peaks corresponding to the transitions from the  $m_s = +\frac{1}{2}$  states of  $A^0X$  drop rapidly with increase of  $B$ . At a temperature of  $\sim 2 \text{ K}$ , these PL peaks disappear from the spectra of  $Al^0X$  and  $Ga^0X$  at  $B > 4 \text{ T}$ , indicating that the spin relaxation time  $\tau_s$  is shorter than the lifetime of  $Al^0X$  or  $Ga^0X$ . Transitions from the  $m_s = +\frac{1}{2}$   $A^0X$  states are still present in the  $In^0X$  and  $Tl^0X$  Zeeman spectra in magnetic fields up to 14.5 T, showing little sign of thermalization. The lifetime<sup>28</sup> of  $In^0X$  (2.5 ns) and  $Tl^0X$  (0.29 ns) must be shorter than  $\tau_s$ , and hence the population of the  $m_s = +\frac{1}{2}$   $A^0X$  level is far from thermal equilibrium. Similarly, little thermalization takes place between the VO states of  $In^0X$  and  $Tl^0X$ . The phonon-assisted intervalley scattering must be a relatively slow process on the scale of the  $In^0X$  or  $Tl^0X$  lifetime.

TABLE I. Selection rules for the optical transitions from  $A^0X$  with holes in the  $J=0$  state, and electron in the VO state  $\phi^{(n)}$  [Eqs. (6), (13), (14), and (22)] with the spin projection  $m_s$  on the [001] crystal axis to  $A^0$  with the [001] angular momentum projection  $m_j$ . Oscillator strengths of the transitions are proportional to the squares of the absolute values of the dipole momentum matrix elements shown as linear combinations of the three independent constants  $\eta$ ,  $\gamma$ , and  $\lambda$ .  $e_x$ ,  $e_y$ , and  $e_z$  are the projections of the luminescence polarization vector  $\mathbf{e}$  on the crystal cubic axes [100], [010], and [001].  $e_+ \equiv e_x + ie_y$ ,  $e_- \equiv e_x - ie_y$ .

$m_s$	$m_j$	$\phi^{(1x)}$	$\phi^{(1z)}$	$\phi^{(32)}$	$\phi_{[001]}^{(5+)}$	$\phi_{[001]}^{(5-)}$	$\phi^{(5z)}$
$+\frac{1}{2}$	$+\frac{3}{2}$	$-\frac{\eta+\lambda}{\sqrt{2}}e_-$	$-\eta e_-$	$\frac{\eta-\lambda}{\sqrt{2}}e_+$	0	$-\sqrt{2}\gamma e_z$	$-\gamma e_+$
$+\frac{1}{2}$	$+\frac{1}{2}$	$-\frac{4i}{\sqrt{6}}\eta e_z$	$-\frac{2i}{\sqrt{3}}\lambda e_z$	0	$i\sqrt{\frac{2}{3}}\gamma e_-$	$-i\sqrt{\frac{2}{3}}\gamma e_+$	0
$+\frac{1}{2}$	$-\frac{1}{2}$	$-\frac{\eta+\lambda}{\sqrt{6}}e_+$	$-\frac{1}{\sqrt{3}}\eta e_+$	$\frac{\eta-\lambda}{\sqrt{6}}e_-$	$\sqrt{\frac{2}{3}}\gamma e_z$	0	$\frac{1}{\sqrt{3}}\gamma e_-$
$+\frac{1}{2}$	$-\frac{3}{2}$	0	0	0	0	0	0
$-\frac{1}{2}$	$+\frac{3}{2}$	0	0	0	0	0	0
$-\frac{1}{2}$	$+\frac{1}{2}$	$i\frac{\eta+\lambda}{\sqrt{6}}e_-$	$\frac{i}{\sqrt{3}}\eta e_-$	$-i\frac{\eta-\lambda}{\sqrt{6}}e_+$	0	$i\sqrt{\frac{2}{3}}\gamma e_z$	$\frac{i}{\sqrt{3}}\gamma e_+$
$-\frac{1}{2}$	$-\frac{1}{2}$	$-\frac{4}{\sqrt{6}}\eta e_z$	$-\frac{2}{\sqrt{3}}\lambda e_z$	0	$\sqrt{\frac{2}{3}}\gamma e_-$	$-\sqrt{\frac{2}{3}}\gamma e_+$	0
$-\frac{1}{2}$	$-\frac{3}{2}$	$i\frac{\eta+\lambda}{\sqrt{2}}e_+$	$i\eta e_+$	$-i\frac{\eta-\lambda}{\sqrt{2}}e_-$	$-i\sqrt{2}\gamma e_z$	0	$-i\gamma e_-$

TABLE II. Selection rules for the optical transitions from  $A^0X$  with holes in the  $J=0$  state, and electron in the VO state  $\phi^{(n)}$  [Eqs. (5), (6), and (23)] with the spin projection  $m'_s$  on the [111] crystal axis to  $A^0$  with the approximate [111] angular momentum projection  $m'_j$ .  $e'_x = (1/\sqrt{6})(e_x + e_y - 2e_z)$ ,  $e'_y = (1/\sqrt{2})(-e_x + e_y)$ ,  $e'_z = (1/\sqrt{3})(e_x + e_y + e_z)$ .  $e'_+ \equiv e'_x + ie'_y$ ,  $e'_- \equiv e'_x - ie'_y$ .

$m'_s$	$m'_j$	$\phi^{(1)}$	$\phi^{(31)}$	$\phi^{(32)}$	$\phi_{[111]}^{(5+)}$	$\phi_{[111]}^{(5-)}$	$\phi_{[111]}^{(50)}$
$+\frac{1}{2}$	$+\frac{3}{2}$	$-\frac{1}{\sqrt{3}}(2\eta+\lambda)e'_-$	$\frac{\eta-\lambda}{\sqrt{6}}(e'_+ - \sqrt{2}e'_z)$	$i\frac{\eta-\lambda}{\sqrt{6}}(e'_+ + \sqrt{2}e'_z)$	$i\sqrt{\frac{2}{3}}\gamma e'_z$	$\frac{2i}{\sqrt{3}}\gamma e'_+$	$\frac{i}{\sqrt{3}}\gamma e'_-$
$+\frac{1}{2}$	$+\frac{1}{2}$	$-\frac{2i}{3}(2\eta+\lambda)e'_z$	$-\frac{2i}{3}(\eta-\lambda)e'_x$	$-\frac{2i}{3}(\eta-\lambda)e'_y$	$-\frac{\sqrt{2}}{3}\gamma e'_+$	$-\frac{\sqrt{2}}{3}\gamma e'_-$	$\frac{4}{3}\gamma e'_z$
$+\frac{1}{2}$	$-\frac{1}{2}$	$-\frac{1}{3}(2\eta+\lambda)e'_+$	$\frac{\eta-\lambda}{3\sqrt{2}}(e'_- - \sqrt{2}e'_z)$	$-i\frac{\eta-\lambda}{3\sqrt{2}}(e'_- + \sqrt{2}e'_z)$	$\frac{2i}{3}\gamma e'_-$	$i\frac{\sqrt{2}}{3}\gamma e'_z$	$\frac{i}{3}\gamma e'_+$
$+\frac{1}{2}$	$-\frac{3}{2}$	0	0	0	0	0	0
$-\frac{1}{2}$	$+\frac{3}{2}$	0	0	0	0	0	0
$-\frac{1}{2}$	$+\frac{1}{2}$	$\frac{i}{3}(2\eta+\lambda)e'_-$	$-i\frac{\eta-\lambda}{3\sqrt{2}}(e'_+ - \sqrt{2}e'_z)$	$\frac{\eta-\lambda}{3\sqrt{2}}(e'_+ + \sqrt{2}e'_z)$	$\frac{\sqrt{2}}{3}\gamma e'_z$	$\frac{2}{3}\gamma e'_+$	$\frac{1}{3}\gamma e'_-$
$-\frac{1}{2}$	$-\frac{1}{2}$	$-\frac{2}{3}(2\eta+\lambda)e'_z$	$-\frac{2}{3}(\eta-\lambda)e'_x$	$-\frac{2}{3}(\eta-\lambda)e'_y$	$i\frac{\sqrt{2}}{3}\gamma e'_+$	$i\frac{\sqrt{2}}{3}\gamma e'_-$	$-\frac{4i}{3}\gamma e'_z$
$-\frac{1}{2}$	$-\frac{3}{2}$	$\frac{1}{\sqrt{3}}(2\eta+\lambda)e'_+$	$-i\frac{\eta-\lambda}{\sqrt{6}}(e'_- - \sqrt{2}e'_z)$	$-i\frac{\eta-\lambda}{\sqrt{6}}(e'_- + \sqrt{2}e'_z)$	$\frac{2}{\sqrt{3}}\gamma e'_-$	$\sqrt{\frac{2}{3}}\gamma e'_z$	$\frac{1}{\sqrt{3}}\gamma e'_+$

TABLE III. Selection rules for the optical transitions from  $A^0X$  with holes in the  $J^{hh}=0$  state, and electron in the VO state  $\phi^{(n)}$  [Eqs. (6), (13), (14), (27), and (28)] with the spin projection  $m_s''$  on the  $[110]$  crystal axis to  $A^0$  with the  $[110]$  momentum projection  $m_j''$ .  $e_x'' = -e_z$ ,  $e_y'' = (1/\sqrt{2})(-e_x + e_y)$ ,  $e_z'' = (1/\sqrt{2})(e_x + e_y)$ .  $e_+'' \equiv e_x'' + ie_y''$ ,  $e_-'' \equiv e_x'' - ie_y''$ .

$m_s''$	$m_j''$	$\phi^{(1x)}$	$\phi^{(1z)}$	$\phi^{(32)}$	$\phi_{[110]}^{(5x'')}$	$\phi_{[110]}^{(5y'')}$	$\phi_{[110]}^{(5z'')}$
$+\frac{1}{2}$	$+\frac{3}{2}$	$-\frac{1}{\sqrt{2}}(\eta e_-'' + \eta e_x'' - i\lambda e_y'')$	$-\lambda e_x'' + i\eta e_y''$	$\frac{i}{\sqrt{2}}(\eta - \lambda)e_z''$	$-\gamma e_y''$	$-\gamma e_+''$	$i\gamma e_z''$
$+\frac{1}{2}$	$+\frac{1}{2}$	$-\frac{2i}{\sqrt{6}}(\eta + \lambda)e_z''$	$-\frac{2i}{\sqrt{3}}\eta e_z''$	$-\frac{2i}{\sqrt{6}}(\eta - \lambda)e_y''$	$-\frac{2}{\sqrt{3}}\gamma e_z''$	0	$-\frac{2}{\sqrt{3}}\gamma e_x''$
$+\frac{1}{2}$	$-\frac{1}{2}$	$-\frac{1}{\sqrt{6}}(\eta e_+'' + \eta e_x'' + i\lambda e_y'')$	$-\frac{1}{\sqrt{3}}(\lambda e_x'' + i\eta e_y'')$	$-\frac{i}{\sqrt{6}}(\eta - \lambda)e_z''$	$\frac{1}{\sqrt{3}}\gamma e_y''$	$\frac{1}{\sqrt{3}}\gamma e_-''$	$\frac{i}{\sqrt{3}}\gamma e_z''$
$+\frac{1}{2}$	$-\frac{3}{2}$	0	0	0	0	0	0
$-\frac{1}{2}$	$+\frac{3}{2}$	0	0	0	0	0	0
$-\frac{1}{2}$	$+\frac{1}{2}$	$\frac{i}{\sqrt{6}}(\eta e_-'' + \eta e_x'' - i\lambda e_y'')$	$\frac{i}{\sqrt{3}}(\lambda e_x'' - i\eta e_y'')$	$\frac{1}{\sqrt{6}}(\eta - \lambda)e_z''$	$\frac{i}{\sqrt{3}}\gamma e_y''$	$\frac{i}{\sqrt{3}}\gamma e_+''$	$\frac{1}{\sqrt{3}}\gamma e_z''$
$-\frac{1}{2}$	$-\frac{1}{2}$	$-\frac{2}{\sqrt{6}}(\eta + \lambda)e_z''$	$-\frac{2}{\sqrt{3}}\eta e_z''$	$-\frac{2}{\sqrt{6}}(\eta - \lambda)e_y''$	$\frac{2i}{\sqrt{3}}\gamma e_z''$	0	$\frac{2i}{\sqrt{3}}\gamma e_x''$
$-\frac{1}{2}$	$-\frac{3}{2}$	$\frac{i}{\sqrt{2}}(\eta e_+'' + \eta e_x'' + i\lambda e_y'')$	$i\lambda e_x'' - \eta e_y''$	$-\frac{1}{\sqrt{2}}(\eta - \lambda)e_z''$	$-i\gamma e_y''$	$-i\gamma e_-''$	$\gamma e_z''$

Components labeled by asterisks that appear in the  $\text{Al}^0X$  and  $\text{Ga}^0X$  spectra in magnetic fields above 10 T are due to  $J=2$  excited-state components of  $A^0X$  with two-hole momentum projection on the magnetic field of  $M_J=-2$ , and electron spin projection  $m_s = -\frac{1}{2}$ . They show the same VOS and have the same final state  $m_j = -3/2$  as the high-energy components  $c$  originating from the  $J=0$ ,  $m_s = -\frac{1}{2}$   $A^0X$  states. The intensity of these new components increases rapidly when they cross the  $c$  components in the spectra of  $\text{Al}^0X$  at about 11 T. The intensity of the rest of the spectrum drops at the same time apparently due to thermalization of the  $J=0$ ,  $m_s = -\frac{1}{2}$   $A^0X$  state, which becomes higher in energy than the  $J=2$ ,  $M_J=-2$ ,  $m_s = -\frac{1}{2}$  state in strong magnetic fields. We observed no such components for  $\text{In}^0X$  or  $\text{Tl}^0X$ , probably because the zero-field splitting between the  $J=2$  and the  $J=0$  states in  $\text{In}^0X$  and  $\text{Tl}^0X$  is considerably larger than in  $\text{Al}^0X$  and  $\text{Ga}^0X$ .

Figures 10–12 show the photon energies of the PL peaks as a function of  $\langle 001 \rangle$ ,  $\langle 111 \rangle$ , and  $\langle 110 \rangle$  magnetic fields. Dots represent experimental peak positions, curved solid lines show predictions of the theory described above. The letters labeling the PL peaks in Figs. 4–8 and 10–16 correspond to the labels of the allowed optical transitions in Fig. 9 with the subscripts showing the  $A^0X$  VO state as labeled in Fig. 1. Table IV lists the parameters of the theory such as the VOS constants  $\Delta_{15}^{\text{VO}}$ ,  $\Delta_{35}^{\text{VO}}$ , the SOC constant  $\lambda^{\text{SO}}$ , and the ratios of the selection rules constants  $\gamma/\eta$  and  $\lambda/\eta$  that were determined directly from the zero-field spectra. Table V lists the  $g$  factors  $g_e, g_1, g_2$  and the diamagnetic shift constants  $q_0, q_d^e, q_2$ , and  $q_3$  whose values were determined from the best fit to a subset of data in  $\langle 001 \rangle$  and  $\langle 111 \rangle$  fields. The constant  $q_0$  accounts for the difference between the isotropic diamagnetic shifts of  $A^0X$  and  $A^0$ . The theory predicts the peak

energies of all the observed features in the spectra with better than 0.01-meV accuracy in the range of magnetic fields from 0.5 to 14.5 T including the  $\langle 110 \rangle$  data, which have not been used at all in the parameter fitting procedure. It should be noted that it is impossible to match the experimental data in magnetic fields using any assignment of the zero field  $A^0X$  VO states other than that shown in Fig. 2. The ordering of the VO states thus unambiguously follows from the pattern of the diamagnetic VOS in the Zeeman spectra.

The only considerable deviation of the PL peak positions from the theoretical predictions occur at zero field. Theoretical peak positions for  $\text{Al}^0X$ ,  $\text{Ga}^0X$ , and  $\text{In}^0X$  fall approximately in the middle between the two peaks of each doublet observed in the zero-field spectra. This is of course exactly as expected, since the theory does not take into account the zero-field intrinsic splitting of the  $A^0$  ground state. Nonetheless, it predicts with remarkable accuracy the  $A^0X$  transition energies in magnetic fields. Thus, the zero-field  $A^0$  splitting practically does not affect the  $A^0$  energy levels in magnetic fields above 1 T, when the paramagnetic splitting of the  $A^0$  sublevels exceeds the zero-field splitting.

#### D. Polarized Zeeman spectra

Once the parameters of the theory have been determined, it is possible to predict further details of the  $A^0X$  PL spectrum in a particular magnetic field. Figures 13–16 show the experimental (bottom) and the theoretical (top) spectra of  $\text{Al}^0X$  and  $\text{In}^0X$  in  $\langle 001 \rangle$  and  $\langle 111 \rangle$  magnetic fields with luminescence radiation polarized either parallel or perpendicular to the magnetic field. Each PL peak in the theoretical spectra was approximated by a Gaussian with the maximum at the theoretically predicted transition energy and the amplitude

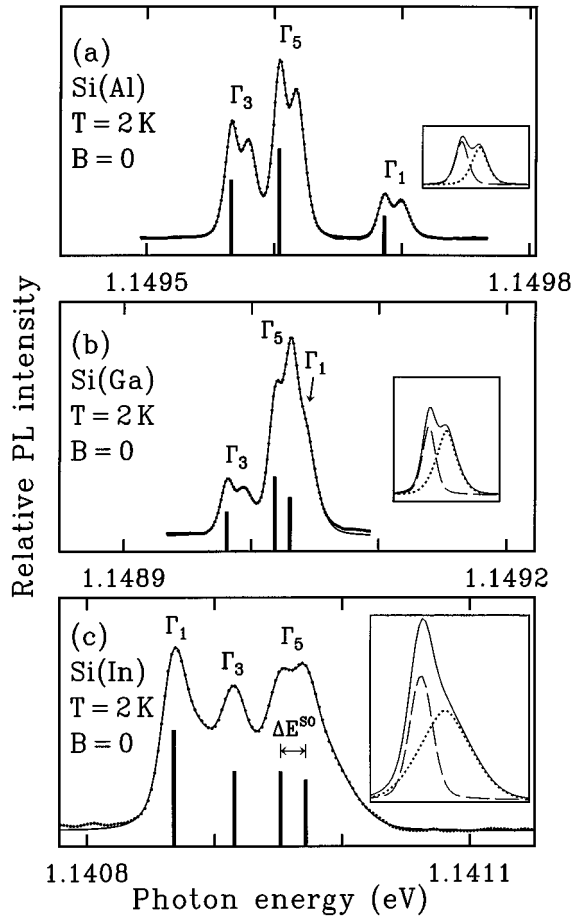


FIG. 2. No-phonon PL spectra of excitons bound to (a) Al, (b) Ga, and (c) In atoms in Si.  $T=2$  K,  $B=0$ . Dots: experiment. Resolution: 0.0025 meV (a),(b), 0.006 meV (c). Solid lines: fits to the data using three (four for In) identical doublets as shown in the right-hand inset for each acceptor. The vertical bars mark the intensity and the energy position of the lower-energy component (dashed line) of each doublet pair used in the fit. The  $\Gamma_5$  state of the In bound exciton (c) is split by the spin-orbit coupling ( $\Delta E^{SO} = \frac{3}{2}\lambda^{SO}$ ).

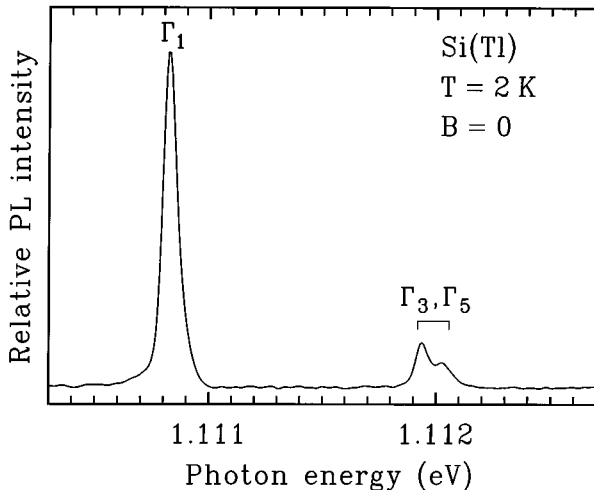


FIG. 3. No-phonon PL spectrum of excitons bound to Tl atoms ( $\text{Tl}^0\text{X}$ ) in Si.  $T=2$  K,  $B=0$ . Resolution: 0.025 meV.

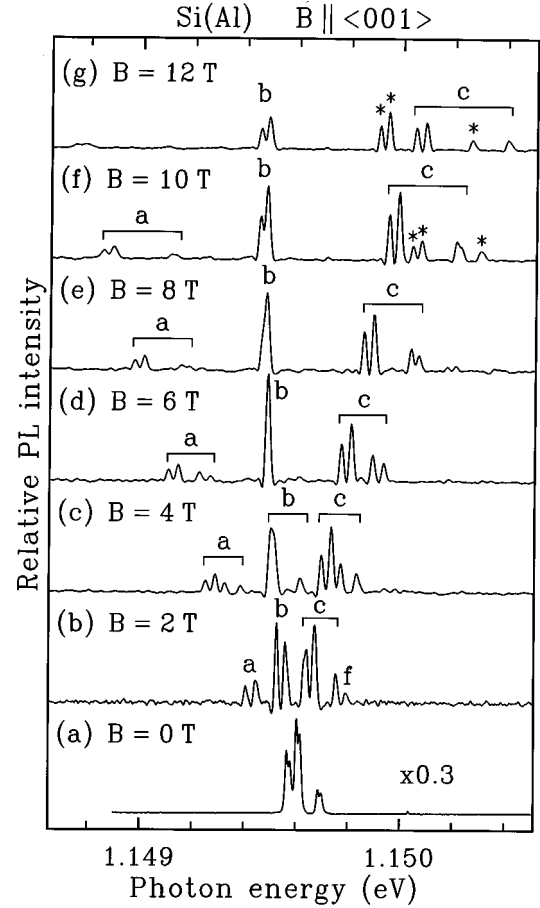


FIG. 4. PL spectra of excitons bound to Al acceptors ( $\text{Al}^0\text{X}$ ) in  $\langle 001 \rangle$  magnetic fields with  $B=0$  (a), 2 T (b), 4 T (c), 6 T (d), 8 T (e), 10 T (f), and 12 T (g). Voigt configuration,  $T=2$  K, resolution 0.012 meV (b)–(g). Asterisks label the components due to the  $J=2$ ,  $M_j=-2$  two-hole state of  $\text{Al}^0\text{X}$ .

calculated on the basis of the selection rules listed in Tables I and II. The amplitude ratios in the  $\langle 110 \rangle$  Zeeman spectra depend on the crystallographic direction in which PL radiation is emitted from the sample, as follows from the selection rules listed in Table III, and we did not measure the polarized  $\langle 110 \rangle$  Zeeman spectra.

The theoretical spectra have been calculated for the  $\text{A}^0\text{X}$  VO states corresponding to the infinite  $B$  limit and assuming complete thermalization of the  $\text{Al}^0\text{X}$  energy levels and no thermalization at all for  $\text{In}^0\text{X}$ . In view of these approximations and some degree of depolarization in experimental spectra, the theory predicts the  $\text{A}^0\text{X}$  Zeeman spectra quite adequately. In particular, it accounts nicely for the small shifts of the  $\Gamma_5$  spectral components due to SOC in  $\text{In}^0\text{X}$  Zeeman spectra. For example, the energy separation of the PL peak  $d_{5-}$  from the peak  $d_{32}$  in the experimental  $\langle 001 \rangle$  Zeeman spectrum (Fig. 14) is smaller than the separation of the  $a_{5-}$  peak from the  $a_{32}$  peak due to the SOC term  $-\lambda^{SO}/2$  in Eqs. (24) and (25).

Experimental polarized Zeeman spectra of  $\text{Ga}^0\text{X}$  (not shown) similarly well agreed with the theoretical predictions. The  $\text{Tl}^0\text{X}$  PL (Fig. 8) was only weakly polarized in magnetic fields and we made only qualitative comparison with

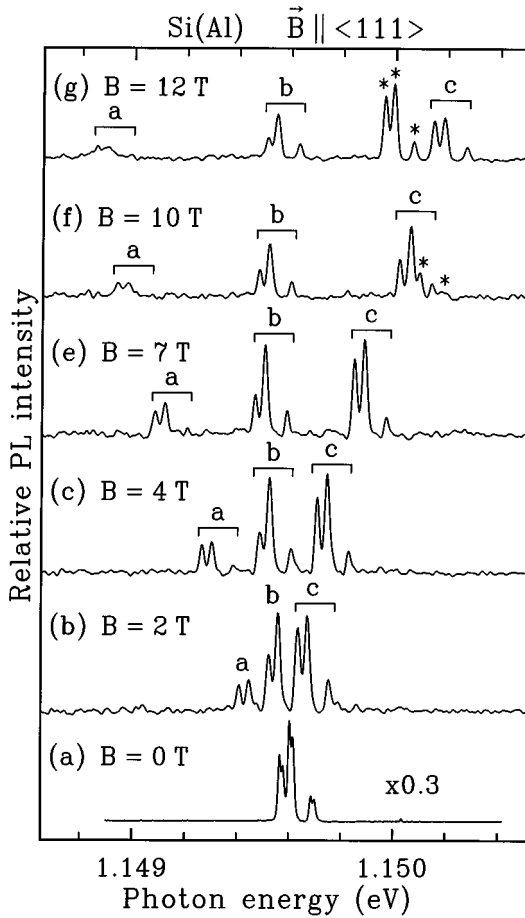


FIG. 5. PL spectra of  $\text{Al}^0\text{X}$  in  $\langle 111 \rangle$  magnetic fields with  $B=0$  (a), 2 T (b), 4 T (c), 7 T (e), 10 T (f), and 12 T (g). Voigt configuration,  $T=2$  K.

the theory, which confirmed that the  $\Gamma_1$  VO state of  $\text{Tl}^0\text{X}$  has the lowest energy at zero field.

#### IV. DISCUSSION

Our high-resolution Zeeman-effect measurements furnish a wide variety of useful information about  $A^0$  and  $A^0\text{X}$  in silicon. In particular, a very good agreement between our simple theoretical treatment of  $A^0$  and  $A^0\text{X}$  and experimental results shows that the single-particle approximation provides an adequate description of  $A^0\text{X}$  in magnetic fields up to 14.5 T, and confirms that the holes occupy the  $J=0$  state in the ground state of  $\text{Al}^0\text{X}$ ,  $\text{Ga}^0\text{X}$ ,  $\text{In}^0\text{X}$ , and  $\text{Tl}^0\text{X}$  at zero field.

The pattern of diamagnetic shifts and diamagnetic splittings of the PL components in magnetic fields with  $\langle 001 \rangle$  and  $\langle 110 \rangle$  orientations (Figs. 10–12) provides a unique signature for each VO state of  $A^0\text{X}$ , thus allowing unambiguous identification of the VO states in the zero-field spectra (except for  $\text{Tl}^0\text{X}$  where VOS is too big and diamagnetic splittings are too small to distinguish between the  $\Gamma_3$  and the  $\Gamma_5$  VO states). The VOS measured in this way and listed in Table IV exhibit consistent trends with increasing of the  $A^0$  ionization energy  $E_I$ .

The splitting between the  $\Gamma_3$  and the  $\Gamma_5$  VO states, whose wave functions have a node in the central cell region, does not change very much from B to In with the  $\Gamma_5$  state slightly

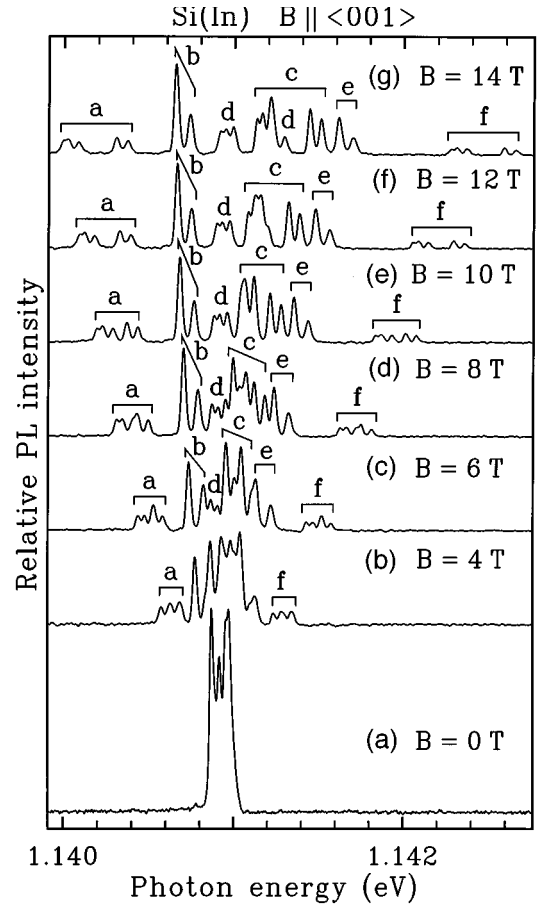


FIG. 6. PL spectra of excitons bound to In acceptors ( $\text{In}^0\text{X}$ ) in  $\langle 001 \rangle$  magnetic fields with  $B=0$  (a), 4 T (b), 6 T (c), 8 T (d), 10 T (e), 12 T (f), and 14 T (g). Voigt configuration,  $T=2$  K.

(0.03–0.05 meV) higher than the  $\Gamma_3$  state. The energy of the VO state  $\Gamma_1$ , on the other hand, is getting progressively lower relative to the states  $\Gamma_3$  and  $\Gamma_5$  with the increase of  $E_I$ . Moreover, the  $\Gamma_1$  state is shallower than the states  $\Gamma_3$  and  $\Gamma_5$  in  $\text{B}^0\text{X}$ ,  $\text{Al}^0\text{X}$ , and  $\text{Ga}^0\text{X}$ , deeper in  $\text{In}^0\text{X}$ , and much deeper in  $\text{Tl}^0\text{X}$ . This trend may be explained by stronger localization of holes in  $A^0\text{X}$  with increasing  $E_I$  of  $A^0$ . The negatively charged acceptor ion  $A^-$  repels the electron in  $A^0\text{X}$ , which may increase the relative energy of the  $\Gamma_1$  VO state for shallower  $A^0$  if the local positive charge density due to the holes is low in the vicinity of the central cell (the  $\Gamma_1$  electron penetrates more into the central cell region, which has a negative net charge). For deeper acceptors, the holes move closer to  $A^-$ , and screen more effectively its negative charge from the electron. Then, the  $\Gamma_1$  electron may interact more effectively with the holes rather than with  $A^-$ , resulting in increased binding energy relative to the  $\Gamma_3$  and the  $\Gamma_5$  states. In the limit of the very deep acceptor Tl, the holes in  $\text{Tl}^0\text{X}$  must be almost completely screening  $\text{Tl}^-$  from the electron, justifying the ‘‘pseudodonor’’ analogy for  $\text{Tl}^0\text{X}$ .

The monotonic reduction of the diamagnetic shift constant  $q_0$  (Table V) with the increase of  $E_I$  also indicates that the average radius  $R_{A^0\text{X}}$  of  $A^0\text{X}$ , which is proportional to  $\sqrt{q_0}$  is getting smaller when  $A^0$  gets deeper. However, the change of  $R_{A^0\text{X}}$  is not as significant as one could expect from  $E_I$ . For example,  $R_{A^0\text{X}}$  decreases only by 10% from Al to In

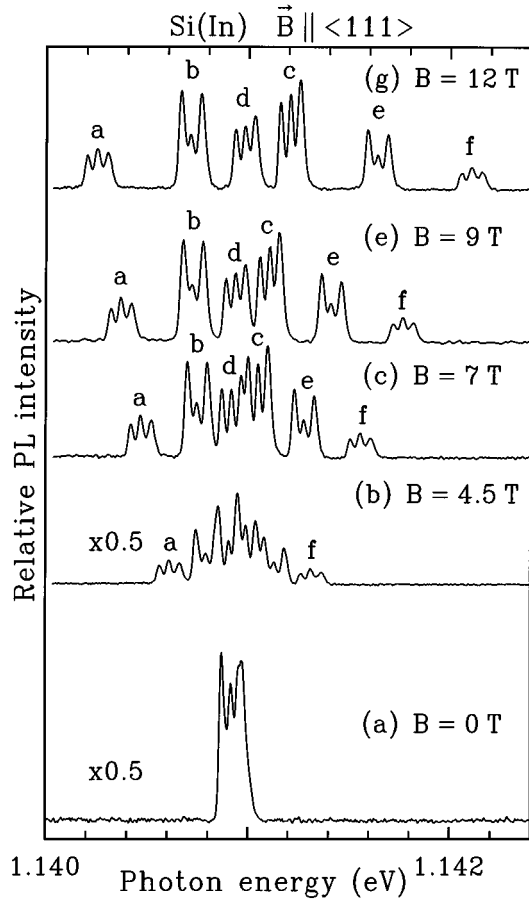


FIG. 7. PL spectra of  $\text{In}^0X$  in  $\langle 111 \rangle$  magnetic fields with  $B=0$  (a), 4.5 T (b), 7 T (c), 9 T (e), and 12 T (g). Voigt configuration,  $T=2$  K.

while  $E_I$  more than doubles. The anisotropic diamagnetic shift constant  $q_d^e$  responsible for the diamagnetic splitting of the electron VO states also decreases monotonically with increasing  $E_I$ .

The electron  $g$  factor  $g^e$  has the free-electron value 2.0 for all  $A^0X$  including  $\text{In}^0X$ , where the 0.02-meV spin-orbit splitting of the  $\Gamma_5$  electron states can be treated as a small perturbation. The isotropic  $\Gamma_8$  hole  $g$  factor  $g_1^h$  is very close to 1 for the shallower acceptors B, Al, and Ga. It is smaller for the deeper  $A^0$ , In and Tl, which may be due to the JTE.<sup>29</sup> The hole  $g$  factors are practically isotropic for Al<sup>0</sup> and Ga<sup>0</sup> ( $g_2 \approx 0$ ), indicating very small tetrahedral contribution to the  $\Gamma_8 A^0$  state, which justifies the use of the angular momentum projection  $m_j$  for labeling of the  $A^0$  eigenfunctions, since  $m_j$  under these circumstances is practically a “good” quantum number. The ratio of the anisotropic  $g$  factor  $g_2^h$  to the isotropic  $g_1^h$  increases from In<sup>0</sup> to Tl<sup>0</sup> underscoring the greater influence of the tetrahedral central cell.

Nonthermal populations of the excited spin and VO states of the electron in  $\text{In}^0X$  and  $\text{Tl}^0X$  (Figs. 3, 6–8, 15, 16) show that neither spin relaxation nor valley-orbit relaxation is fast enough to ensure thermal equilibrium between the energy levels of  $\text{In}^0X$  or  $\text{Tl}^0X$  during their lifetime  $\tau$ . The populations of the Al<sup>0</sup> $X$  and Ga<sup>0</sup> $X$  energy levels, on the other hand, are in thermal equilibrium with the crystal. Hence, the average electron-spin relaxation time  $\tau_s$  and the valley-orbit relaxation time  $\tau_{VO}$  in  $A^0X$  must be in the range between the

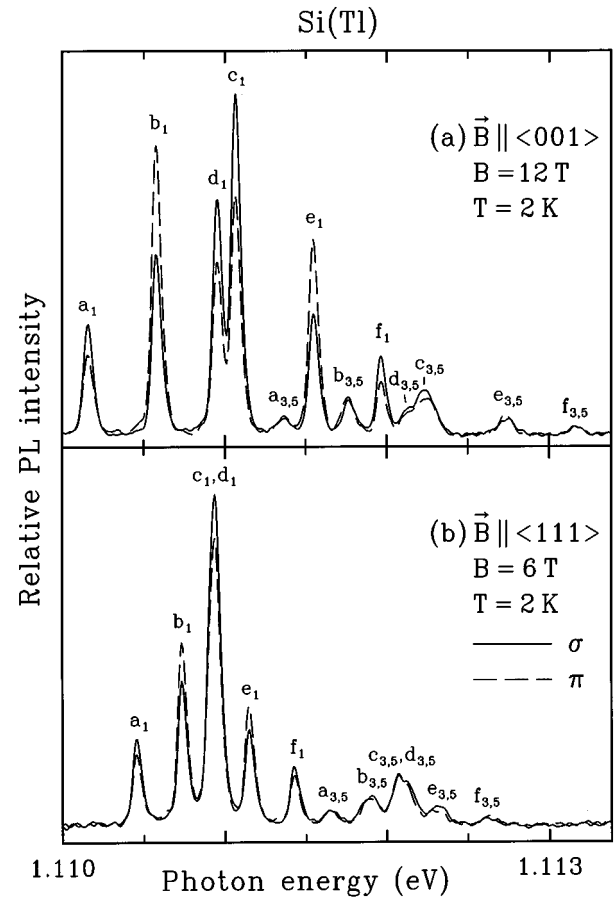


FIG. 8. Spectra of  $\text{Tl}^0X$  PL polarized perpendicular ( $\sigma$ ) and parallel ( $\pi$ ) to the  $\langle 001 \rangle$  (a) and  $\langle 111 \rangle$  (b) magnetic field. Voigt configuration,  $T=2$  K.

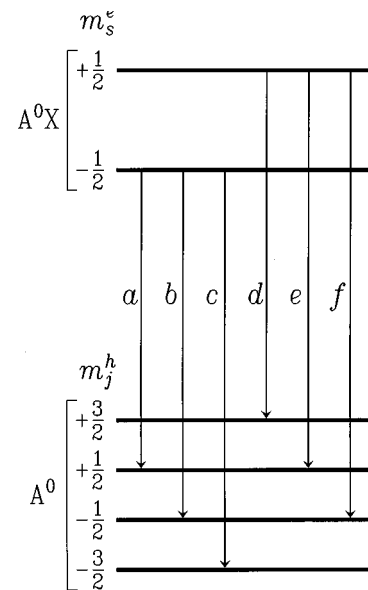


FIG. 9.  $A^0X$  and  $A^0$  energy levels (without VOS) and allowed optical transitions in magnetic fields.  $m_s^e$  is the electron spin projection, and  $m_j^h$  is the approximate hole angular momentum projection on the magnetic field axis.

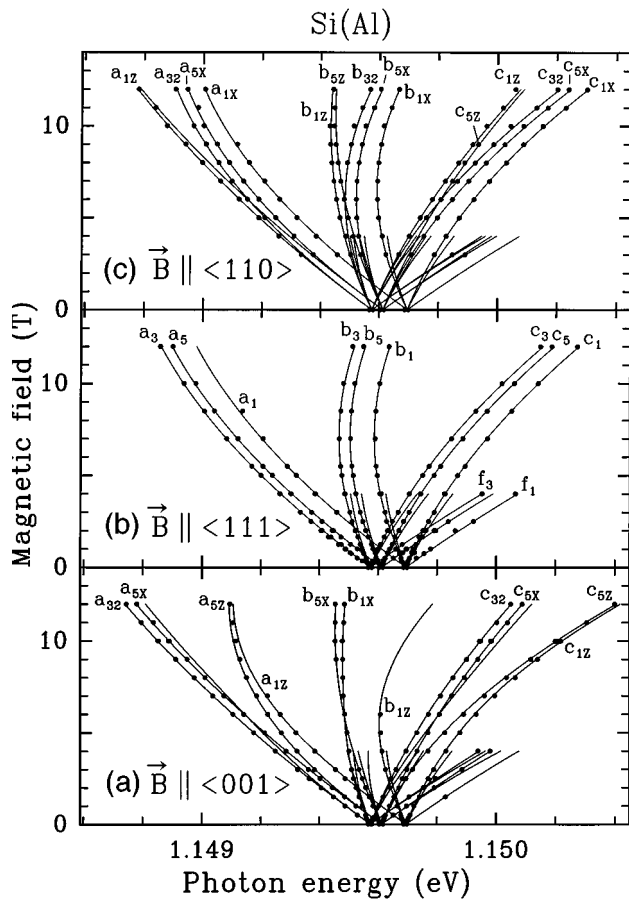


FIG. 10. Experimental (dots) and theoretical (solid lines) positions of the  $\text{Al}^0\text{X}$  PL peaks in  $\langle 001 \rangle$  (a),  $\langle 111 \rangle$  (b), and  $\langle 110 \rangle$  (c) magnetic fields. The peaks are labeled by the same letters as the optical transitions in Fig. 9 with the subscripts indicating the  $\text{Al}^0\text{X}$  valley-orbit (VO) states as in Fig. 1.

lifetimes of  $\text{In}^0\text{X}$  ( $\tau=2.5$  ns) (Ref. 28) and  $\text{Al}^0\text{X}$  ( $\tau=76$  ns) (Ref. 30).

The ratios of the selection rule constants  $\gamma/\eta$  and  $\lambda/\eta$  have been measured directly from the amplitude ratios of the components in the zero-field PL spectra. Nonthermal population of the excited VO states increased the uncertainty in our measurements of these constants since the excited VO states were only partially thermalized, and it was difficult to take thermalization properly into account. Nonetheless, agreement between the amplitude ratios in theoretical and experimental Zeeman spectra is more than qualitative, and some useful information about the dominant radiative electron-hole recombination processes in  $\text{A}^0\text{X}$  can be obtained from experimental values of  $\gamma/\eta$  and  $\lambda/\eta$ .

An indirect optical transition in Si may be considered as a virtual scattering of the electron to the  $\Gamma$  point of the Brillouin zone or of the hole to one of the six  $\Delta$  points corresponding to the conduction-band minimum followed by a direct optical transition. The case  $\gamma \neq 0$ ,  $\eta \neq 0$ ,  $\lambda = 0$  corresponds to transitions through the band  $\Delta_5$  (hole scattering), while  $\lambda = \eta$  and  $\gamma = 0$  correspond to transitions through the band  $\Gamma'_2$  (electron scattering).<sup>27</sup> In Table IV,  $\lambda \approx 0$  for all group-III acceptors except for Al, indicating that NP recombination involves predominantly virtual scattering of one of the holes, which is not surprising since the holes in  $\text{A}^0\text{X}$  interact more strongly

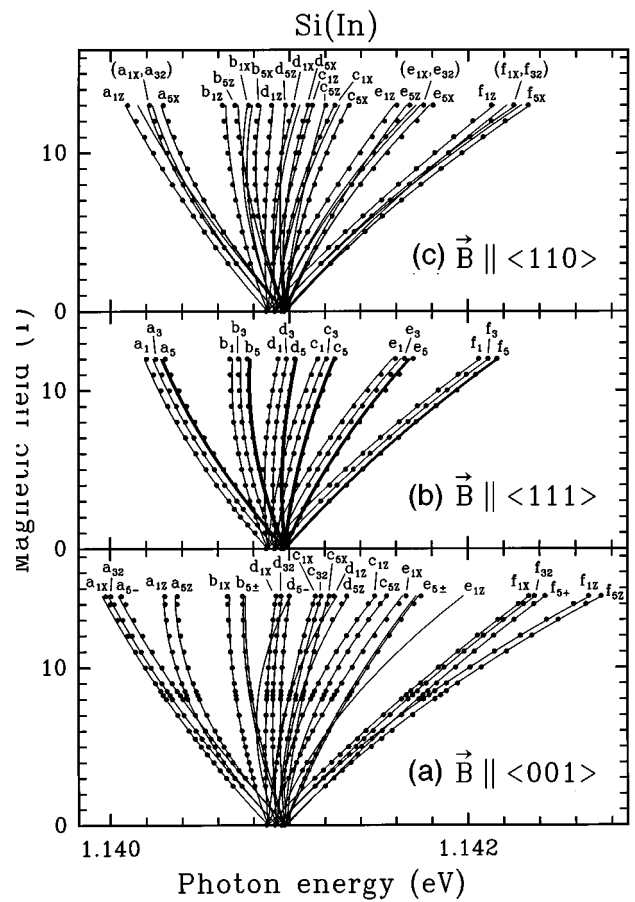


FIG. 11. Experimental (dots) and theoretical (solid lines) positions of the  $\text{In}^0\text{X}$  PL peaks in  $\langle 001 \rangle$  (a),  $\langle 111 \rangle$  (b), and  $\langle 110 \rangle$  (c) magnetic fields.

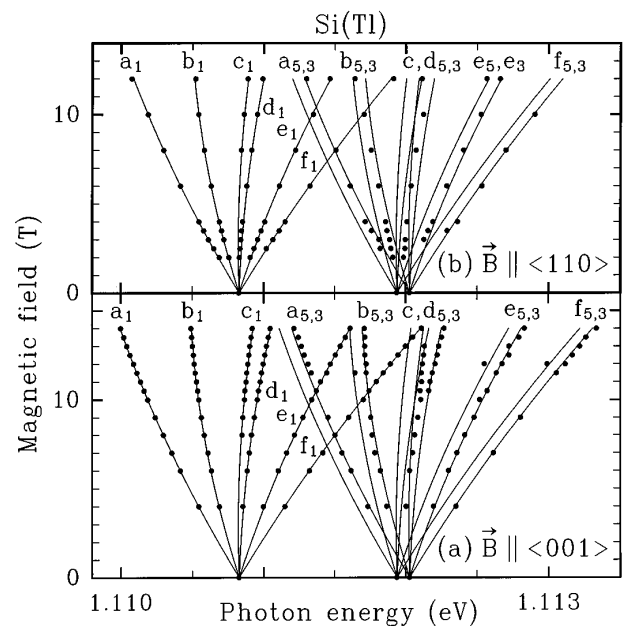


FIG. 12. Experimental (dots) and theoretical (solid lines) positions of the  $\text{Tl}^0\text{X}$  PL peaks in  $\langle 001 \rangle$  (a),  $\langle 111 \rangle$  (b), and  $\langle 110 \rangle$  (c) magnetic fields.

TABLE IV. Ionization energies  $E_I$  of the group-III acceptors in Si, as well as exciton binding energies  $E_b$  ( $J=0$  two-hole state,  $\Gamma_1$  valley-orbit state), bound exciton lifetimes  $\tau$ , the valley-orbit splittings  $\Delta_{15}^{\text{VO}}$ ,  $\Delta_{35}^{\text{VO}}$ , the spin-orbit coupling constants  $\lambda^{\text{SO}}$ , and the ratios  $\gamma/\eta$ ,  $\lambda/\eta$  of the selection rule constants for excitons bound to these acceptors.

Acceptor	B	Al	Ga	In	Tl
$E_I$ (meV)	45.71 <sup>a</sup>	70.18 <sup>a</sup>	74.05 <sup>a</sup>	156.90 <sup>a</sup>	246 <sup>b</sup>
$E_b$ (meV)	3.7±0.1	4.69±0.05	5.35±0.05	13.51±0.05	43.5±0.1
$\tau$ (ns)	1055 <sup>c</sup>	76 <sup>c</sup>	77 <sup>c</sup>	2.5 <sup>d</sup>	0.29 <sup>d</sup>
$\Delta_{15}^{\text{VO}}$ (meV)	0.032 <sup>e</sup>	0.083±0.001	0.012±0.004	-0.097±0.003	-1.21±0.01 <sup>f</sup> (-1.11±0.01) <sup>g</sup>
$\Delta_{35}^{\text{VO}}$ (meV)	-0.026 <sup>e</sup>	-0.038±0.001	-0.038±0.002	-0.049±0.003	-0.10±0.01 <sup>f</sup> (+0.10±0.01) <sup>g</sup>
$\lambda^{\text{SO}}$ (meV)				0.013±0.003	
$\gamma/\eta$	0.64±0.10	1.06±0.10	1.00±0.10	0.83±0.10	0.6±0.3
$\lambda/\eta$	-0.03±0.20	-0.33±0.20	0.03±0.20	-0.06±0.20	-0.1±0.3

<sup>a</sup>After Ramdas and Rodrigues (Ref. 16).

<sup>b</sup>After W. Scott and J. L. Schmit, Appl. Phys. Lett. **33**, 295 (1978).

<sup>c</sup>After Schmid (Ref. 30).

<sup>d</sup>After Steiner and Thewalt (Ref. 28).

<sup>e</sup>For the  $J=2, M_J=-2$  state of  $\text{B}^0\text{X}$ . After Karasyuk, Brake, and Thewalt (Ref. 14).

<sup>f</sup>If in  $\text{Tl}^0\text{X}$  the  $\Gamma_3$  VO state has lower energy than the  $\Gamma_5$  state.

<sup>g</sup>If in  $\text{Tl}^0\text{X}$  the  $\Gamma_3$  VO state has higher energy than the  $\Gamma_5$  state.

with the central cell potential than does the electron. The nonzero value of  $\lambda$  for Al indicates that in  $\text{Al}^0\text{X}$  virtual scattering of the electron also contributes to NP optical recombination. This correlates with the relatively high VO splitting, due to more effective interaction of the electron in  $\text{Al}^0\text{X}$  with the central cell.

This study, together with our previous<sup>14</sup> one on  $\text{B}^0\text{X}$  PL, demonstrates a rather complete understanding of the  $\text{A}^0\text{X}$  ground state and its transitions, including their fine structure and Zeeman splittings and shifts, for group-III acceptors in Si. As such it provides the most complete description of the properties of acceptor bound excitons in any indirect-gap semiconductor. We plan to complete this work in the near future with the publication of detailed, high-resolution studies of PL of  $\text{A}^0\text{X}$  in Si as a function of uniaxial strains. Still missing, however, is a determination of the existence and magnitude of any intrinsic ground-state splitting for  $\text{Tl}^0$ . The very limited availability (and quality) of Tl-doped Si has prevented any clear resolution of this issue at the present time.

## ACKNOWLEDGMENTS

This work was supported partly by the Natural Sciences and Engineering Research Council of Canada and by the Science and Engineering Research Council (United Kingdom).

## APPENDIX

In this appendix we derive the selection rules for the dipole optical transitions in  $\text{A}^0\text{X}$ , using Kirczenow's<sup>11</sup> theory of NP radiative recombination of BE's in indirect-gap semiconductors, and the selection rules for the radiative decay of free excitons (FE) in Si derived by Pikus<sup>31</sup> on the basis of the symmetry considerations.

The probability of a dipole optical transition from a quantum state  $\Psi_n$  to a state  $\Psi_m$  is proportional to  $|\mathbf{e} \cdot \mathbf{D}_{mn}|^2$ , where  $\mathbf{e}$  is the unit polarization vector of radiation and

$$\mathbf{D}_{mn} = \langle \Psi_m | \mathbf{Q} | \Psi_n \rangle \quad (\text{A1})$$

TABLE V. The  $g$  factors and the diamagnetic shift constants for the group-III  $\text{A}^0$  and  $\text{A}^0\text{X}$ .

Acceptor	B	Al	Ga	In	Tl
$g^e$	1.95 <sup>a</sup>	2.01±0.01	2.00±0.01	2.00±0.01	1.99±0.02
$g_1^h$	1.03 <sup>b</sup>	0.98±0.01	0.96±0.01	0.86±0.01	0.60±0.02
$g_2^h$	0.04 <sup>b</sup>	-0.01±0.01	-0.01±0.01	-0.05±0.01	0.05±0.02
$q_0$ ( $\mu\text{eV/T}^2$ )	2.34 <sup>a</sup>	2.16±0.05	2.04±0.05	1.80±0.05	1.18±0.10
$q_d^e$ ( $\mu\text{eV/T}^2$ )	2.96 <sup>a</sup>	2.19±0.05	1.58±0.05	1.53±0.05	≤0.6
$q_2^h$ ( $\mu\text{eV/T}^2$ )	0.21 <sup>a</sup>	0.11±0.05	0.09±0.05	0.29±0.05	0.20±0.10
$q_3^h$ ( $\mu\text{eV/T}^2$ )	0.07 <sup>a</sup>	-0.03±0.05	-0.02±0.05	-0.01±0.05	-0.03±0.10

<sup>a</sup>After Karasyuk, Brake, and Thewalt (Ref. 14).

<sup>b</sup>After F. Merlet, B. Pajot, Ph. Arcas, and A. M. Jean-Louis, Phys. Rev. B **12**, 3297 (1975).

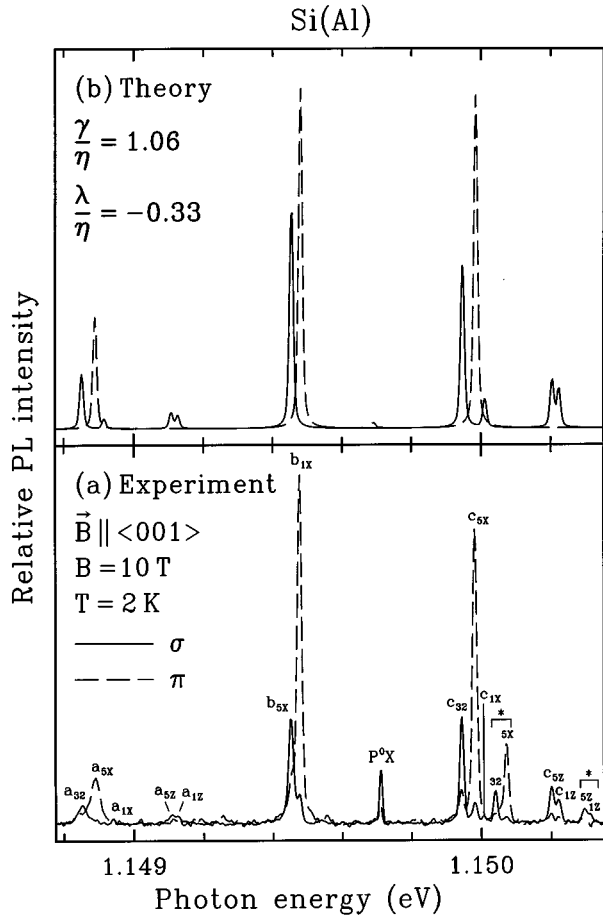


FIG. 13. Experimental (a) and theoretical (b) spectra of  $\text{Al}^0\text{X}$  PL polarized perpendicular ( $\sigma$ ) and parallel ( $\pi$ ) to the  $\langle 001 \rangle$  magnetic field. Voigt configuration.  $B=10$  T. The theoretical spectrum (b) is a convolution of 15 Gaussian peaks centered at the photon energies calculated on the basis of the selection rules listed in Table I. The peaks are labeled by the same letters as the optical transitions in Fig. 9 with the subscripts indicating the  $\text{Al}^0\text{X}$  states as in Fig. 1. Complete thermalization is assumed for the  $m_s = +\frac{1}{2}$   $\text{Al}^0\text{X}$  states. Thermal equilibrium is assumed between the  $\text{Al}^0\text{X}$  VO states at  $T=2$  K. Asterisks label the components due to the  $J=2$ ,  $M_J=-2$  two-hole state of  $A^0\text{X}$ . The PL peak labeled as  $P^0\text{X}$  is due to excitons bound to phosphorus.

is the matrix element of the electric-dipole-momentum operator  $\mathbf{Q}$ .<sup>32</sup> The symmetry of the states  $\Psi_m$  and  $\Psi_n$  determines the relations between the matrix elements  $\mathbf{D}_{mn}$  independent of the particular form of  $\Psi_m$  and  $\Psi_n$ . The number of linearly independent matrix elements is equal to the number of unit representations in the direct product  $(D_\alpha)^* \otimes D_\kappa \otimes D_\beta$  of the representations according to which  $\Psi_m$ ,  $\Psi_n$ , and the components of  $\mathbf{Q}$  transform. In the case of NP optical transitions from  $A^0\text{X}$  to  $A^0$  in Si,  $D_\alpha = \Gamma_8$ ,  $D_\kappa = \Gamma_5$ ,  $D_\beta = (\Gamma_1 + \Gamma_3 + \Gamma_5) \otimes \Gamma_6$ , and the number of linearly independent components of  $\mathbf{D}_{mn}$  is 6. However, this number can be reduced substantially if we adopt the shell model<sup>11</sup> representation for the  $A^0\text{X}$  wave function as an antisymmetrized product of single-particle functions. According to Kirczenow,<sup>11</sup> the two-hole wave function  $\Psi_{hh}$  corresponding to the state  $J=0$  can be presented as

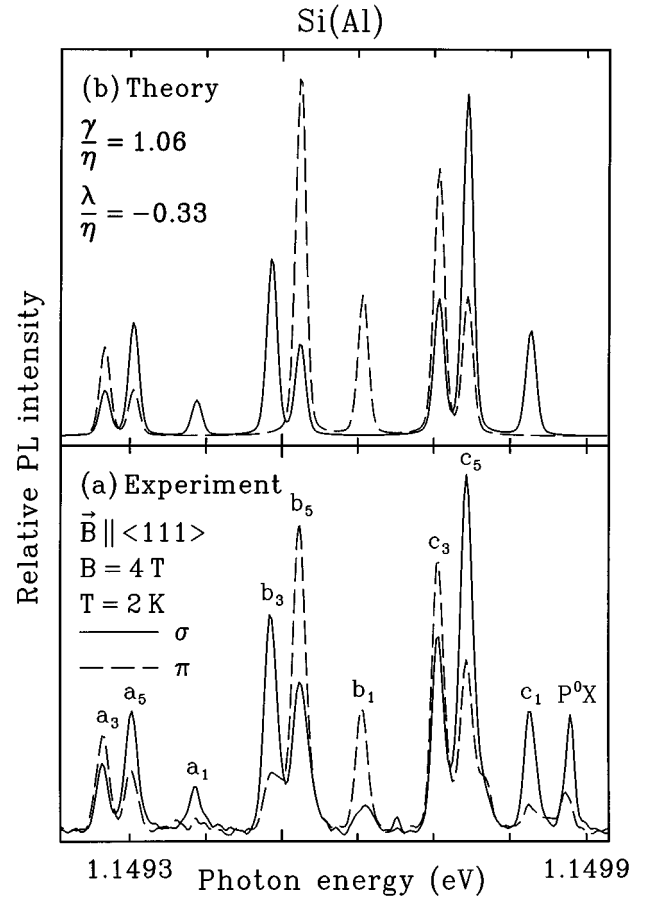


FIG. 14. Experimental (a) and theoretical (b) spectra of  $\text{Al}^0\text{X}$  PL polarized perpendicular ( $\sigma$ ) and parallel ( $\pi$ ) to the  $\langle 111 \rangle$  magnetic field. Voigt configuration.  $B=4$  T. Theoretical spectrum (b) is a convolution of nine Gaussian peaks centered at the photon energies determined from Eqs. (1) and (15)–(19) with relative amplitudes calculated on the basis of the selection rules listed in Table II. Complete thermalization is assumed for the  $m_s = +\frac{1}{2}$   $\text{Al}^0\text{X}$  states. Thermal equilibrium is assumed between the  $\text{Al}^0\text{X}$  VO states at  $T=2$  K.

$$\Psi_{hh}^{\Gamma_1} = -\frac{1}{2} u_{-3/2}(\mathbf{r}_1) u_{+3/2}(\mathbf{r}_2) + \frac{1}{2} u_{-1/2}(\mathbf{r}_1) u_{+1/2}(\mathbf{r}_2) + \frac{1}{2} u_{-3/2}(\mathbf{r}_2) u_{+3/2}(\mathbf{r}_1) - \frac{1}{2} u_{-1/2}(\mathbf{r}_2) u_{+1/2}(\mathbf{r}_1) \quad (\text{A2})$$

where the single-hole functions  $u_\mu$ ,  $\mu = +\frac{3}{2}, +\frac{1}{2}, -\frac{1}{2}, -\frac{3}{2}$ , have the same transformation properties as the  $A^0$  wave functions (1). Following Kirczenow's approach,<sup>11</sup> representation (A2) yields the expression for the dipole matrix elements:

$$\mathbf{D}_{\mu(n)\sigma} \equiv \langle \psi_\mu | \mathbf{Q} | \Psi_{hh}^{\Gamma_1} \phi^{(n)} s_\sigma \rangle = -\frac{1}{2} \rho_{\mu, -3/2} \mathbf{d}_{+3/2, (n)\sigma} + \frac{1}{2} \rho_{\mu, +3/2} \mathbf{d}_{-3/2, (n)\sigma} + \frac{1}{2} \rho_{\mu, -1/2} \mathbf{d}_{+1/2, (n)\sigma} - \frac{1}{2} \rho_{\mu, +1/2} \mathbf{d}_{-1/2, (n)\sigma}, \quad (\text{A3})$$

where  $s_\sigma$  is a spinor  $\frac{1}{2}$ ,  $\rho_{\mu\nu} \equiv \langle \psi_\mu | v_\nu \rangle$  is the overlap integral of the single-hole functions  $\psi_\mu$  and  $v_\nu$ , and  $\mathbf{d}_{\mu(n)\sigma} \equiv \langle \tau u_\mu | \mathbf{Q} | \phi^{(n)} s_\sigma \rangle$  is a dipole momentum matrix ele-

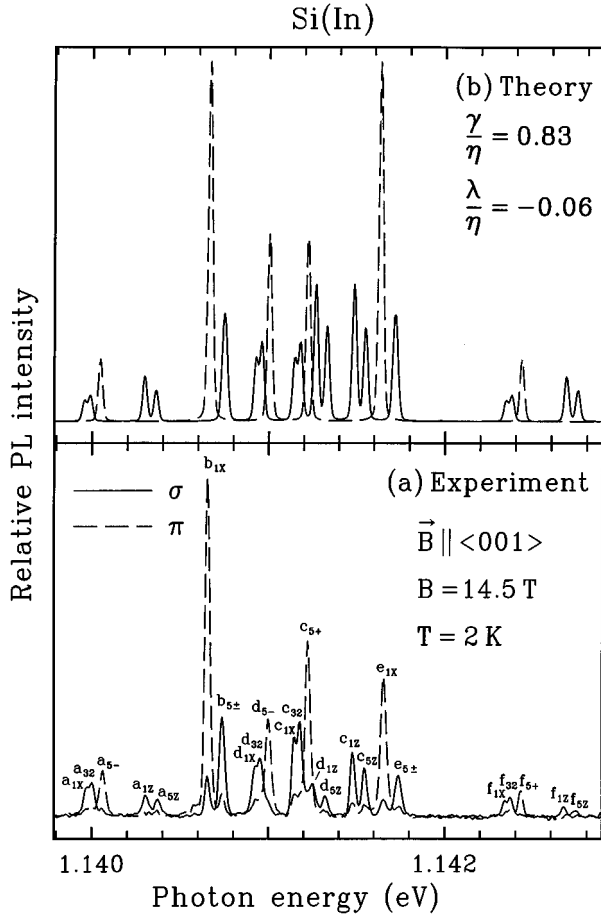


FIG. 15. Experimental (a) and theoretical (b) spectra of  $\text{In}^0\text{X}$  PL polarized perpendicular ( $\sigma$ ) and parallel ( $\pi$ ) to the  $\langle 001 \rangle$  magnetic field. Voigt configuration.  $B=14.5$  T.  $T=2$  K. Theoretical spectrum (b) is a convolution of 36 Gaussian peaks centered at the photon energies determined from Eqs. (1), (15)–(17), and (24)–(26) with relative amplitudes calculated on the basis of the selection rules listed in Table I. Equal populations (no thermalization) are assumed for the spin and VO states of  $\text{In}^0\text{X}$ .

ment for the transition from the single-electron state  $\phi^{(n)}_{s\sigma}$  to the empty single-electron state related to the single-hole state  $u_\mu$  by time reversal (operator  $\tau$ ). Since  $\psi_\mu$  and  $v_\nu$  belong to the same irreducible representation,  $\rho_{\mu\nu}$  is equal to zero for  $\mu \neq \nu$ , and to a constant  $\rho$  independent of the index  $\mu$  otherwise. Thus,  $\mathbf{D}_{\mu(n)}$  is proportional to  $\mathbf{d}_{-\mu,(n)}$  implying that the optical transition from  $A^0\text{X}$  to  $A^0$  can be described in terms of an electron-hole pair recombination:

$$\mathbf{D}_{\mu(n)} = \pm \frac{1}{2} \rho \delta_{\mu\nu} \mathbf{d}_{\nu,(n)}. \quad (\text{A4})$$

Interaction with the short-range central cell potential is crucial for the NP radiative electron-hole recombination in BE.<sup>11</sup> Therefore,  $\mathbf{d}_{\mu,(n)}$  depends predominantly on the behavior of  $\psi_\mu$  and  $v_\nu$  in the central cell region. Hence, as was argued by Kulakovskii, Pikus, and Timofeev,<sup>27</sup> the selection rules for BE should be the same as those for FE (when the effects of the VOS can be neglected). In  $A^0\text{X}$  the VOS is very small, if compared to the binding energy, and the selec-

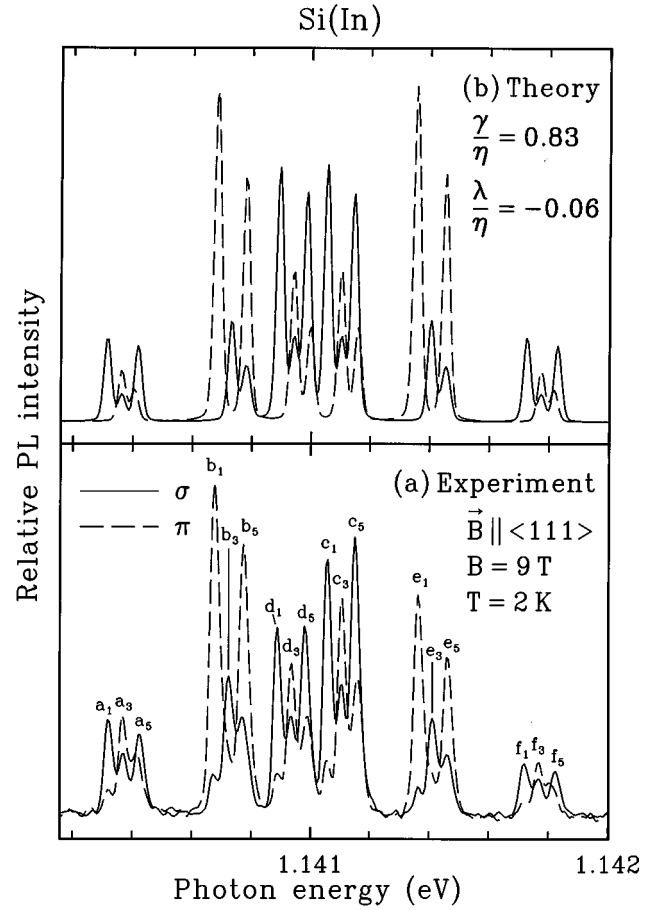


FIG. 16. Experimental (a) and theoretical (b) spectra of  $\text{In}^0\text{X}$  PL polarized perpendicular ( $\sigma$ ) and parallel ( $\pi$ ) to the  $\langle 111 \rangle$  magnetic field. Voigt configuration.  $B=9$  T.  $T=2$  K. Equal populations (no thermalization) are assumed for the spin and VO states of  $\text{In}^0\text{X}$ .

tion rules can still be obtained from the FE selection rules by taking the appropriate linear combinations of the FE dipole matrix elements.

Pikus<sup>31</sup> derived the selection rules for the NP FE recombination related to the interband scattering from substitutional impurities using the methods of group theory. He obtained a simple expression for the matrix  $\mathbf{e} \cdot \mathbf{D}$  in the basis of the spinless hole wave functions  $X, Y, Z$  and the electron wave function  $S$  transforming according to the unit representation of the group of  $\mathbf{k}_z$  ( $z$  valley of the conduction band):

$$\mathbf{e} \cdot \mathbf{D} = \eta(R_x e_x + R_y e_y) + \lambda R_z e_z + i\gamma(R_x e_y + R_y e_x), \quad (\text{A5})$$

where  $\eta$ ,  $\lambda$ , and  $\gamma$  are three real independent constants, and  $R_x$ ,  $R_y$ , and  $R_z$  are three linearly independent matrices, each of which has a single nonzero matrix element  $\langle 0|SX\rangle$ ,  $\langle 0|SY\rangle$ , or  $\langle 0|SZ\rangle$ . A similar expression for the  $\bar{z}$  valley can be obtained by rotation on angle  $\pi$  around the  $x$  axis:

$$\mathbf{e} \cdot \mathbf{D} = \eta(R_x e_x + R_y e_y) + \lambda R_z e_z - i\gamma(R_x e_y + R_y e_x). \quad (\text{A6})$$

A cyclic permutation of (A5) and (A6) yields the dipole ma-

trix elements for the  $x$ ,  $\bar{x}$ ,  $y$ , and  $\bar{y}$  valleys. Linear combinations of these matrix elements with the coefficients determined by the Eq. (4) furnish the expressions for  $\mathbf{d}_{\mu(n)}$  and consequently for  $\mathbf{D}_{\mu(n)}$  listed in the Tables I–III. In these

tables we include the factor  $\frac{1}{5}\rho$  into the constants  $\eta$ ,  $\lambda$ , and  $\gamma$  and use for the [111] and [110] field directions the rotated  $j=3/2$  and  $s=1/2$  bases as given by Bhattacharjee and Rodriguez.<sup>24</sup>

- <sup>1</sup>P. Colley and E. C. Lightowers, *Semicond. Sci. Technol.* **2**, 157 (1987).
- <sup>2</sup>J. R. Haynes, *Phys. Rev. Lett.* **4**, 361 (1960).
- <sup>3</sup>For a review, see P. J. Dean and D. C. Herbert, in *Excitons, Topics in Current Physics Vol 14*, edited by K. Cho (Springer-Verlag, Berlin, 1979), p. 55; M. L. W. Thewalt, in *Excitons*, edited by E. I. Rashba and M. D. Sturge (North-Holland, Amsterdam, 1982), p. 393.
- <sup>4</sup>M. A. Vouk and E. C. Lightowers, in *Proceedings of the Thirteenth International Conference on the Physics of Semiconductors, Rome, 1976*, edited by F. G. Fumi (Tipografia Marves, Rome, 1977), p. 1098.
- <sup>5</sup>M. L. W. Thewalt, *Can. J. Phys.* **55**, 1463 (1977).
- <sup>6</sup>E. C. Lightowers and M. O. Henry, *J. Phys. C* **10**, L247, (1977).
- <sup>7</sup>K. R. Elliott, G. C. Osbourn, D. L. Smith, and T. C. McGill, *Phys. Rev. B* **17**, 1808 (1978).
- <sup>8</sup>E. U. Condon and G. H. Shortley, *The Theory of Atomic Spectra* (Cambridge University Press, Cambridge, 1964).
- <sup>9</sup>F. S. Ham and Chi-Hong Leung, *Phys. Rev. Lett.* **71**, 3186 (1993).
- <sup>10</sup>H. A. Jahn and E. Teller, *Proc. R. Soc. London Ser. A* **161**, 220 (1937).
- <sup>11</sup>G. Kirczenow, *Can. J. Phys.* **55**, 1787 (1977).
- <sup>12</sup>V. A. Karasyuk and Ya. E. Pokrovskii, *Pis'ma Zh. Eksp. Teor. Fiz.* **37**, 537 (1983) [*JETP Lett.* **37**, 640 (1983)].
- <sup>13</sup>M. V. Gorbunov, A. S. Kaminskii, A. N. Safonov, *Zh. Eksp. Teor. Fiz.* **94**, 247 (1988) [*Sov. Phys. JETP* **67**, 355 (1988)].
- <sup>14</sup>V. A. Karasyuk, D. M. Brake, and M. L. W. Thewalt, *Phys. Rev. B* **47**, 9354 (1992).
- <sup>15</sup>G. F. Koster, J. O. Dimmock, R. G. Wheeler, and H. Statz, *Properties of the Thirty-two Point Groups* (MIT Press, Cambridge, MA, 1966).
- <sup>16</sup>See, e.g., A. K. Ramdas and S. Rodrigues, *Rep. Prog. Phys.* **44**, 1297 (1981).
- <sup>17</sup>M. L. W. Thewalt and D. M. Brake, *Mat. Sci. Forum* **65-66**, 187 (1990).
- <sup>18</sup>V. A. Karasyuk, S. An, M. L. W. Thewalt, and E. C. Lightowers, *Phys. Rev Lett.* **73**, 2340 (1994).
- <sup>19</sup>V. A. Karasyuk, S. An, M. L. W. Thewalt, E. C. Lightowers, and A. S. Kaminskii, *Solid State Commun.* **93**, 379 (1995).
- <sup>20</sup>V. A. Karasyuk and S. An, in *Proceedings of the 22nd International Conference on the Physics of Semiconductors, Vancouver, 1994*, edited by D. J. Lockwood (World Scientific, Singapore 1995), p. 2371.
- <sup>21</sup>K. R. Elliott, D. L. Smith, and T. C. McGill, *Solid State Commun.* **27**, 317 (1978).
- <sup>22</sup>V. D. Kulakovskii and A. V. Malyavkin, *Phys. Status Solidi B* **92**, 455 (1979).
- <sup>23</sup>J. Weber, H. Conzelman, and R. Sauer, in *Proceedings of the Fifteenth International Conference on the Physics of Semiconductors, Kyoto, 1980* [*J. Phys. Soc. Jpn. Suppl. A* **49**, 425 (1980)].
- <sup>24</sup>A. K. Bhattacharjee and S. Rodriguez, *Phys. Rev. B* **6**, 3836 (1972).
- <sup>25</sup>A. J. Mayur, M. Dean Sciacca, A. K. Ramdas, and S. Rodriguez, *Phys. Rev. B* **48**, 10 893 (1993).
- <sup>26</sup>G. D. Watkins and F. S. Ham, *Phys. Rev. B* **1**, 4071 (1970).
- <sup>27</sup>V. D. Kulakovskii, G. E. Pikus, and V. B. Timofeev, *Usp. Fiz. Nauk* **135**, 237 (1981) [*Sov. Phys. Usp.* **24**, 815 (1981)].
- <sup>28</sup>T. Steiner and M. L. W. Thewalt, *Solid State Commun.* **49**, 1121 (1984).
- <sup>29</sup>F. S. Ham, in *Electron Paramagnetic Resonance*, edited by S. Geschwind (Plenum, New York, 1972), p. 37.
- <sup>30</sup>W. Schmid, *Phys. Status Solidi B* **84**, 529 (1977).
- <sup>31</sup>G. E. Pikus, *Fiz. Tverd. Tela* **19**, 1653 (1977) [*Sov. Phys. Solid State* **19**, 965 (1977)].
- <sup>32</sup>D. I. Blochintsev, *Quantum Mechanics* (Reidel, Dordrecht, 1964), p. 295.